第百四十五號

（昭和十二年二月發行）

抄　錄

對流の理論的及び實驗的研究と其の海陸風への應用

所員　小林辰男
所員　佐々木達治郎
助手　長内忠雄

第一章　水槽實驗

實驗に使用した水槽は，長さ 3 m. 幅 20 cm. のもので，これに約 30 cm. の深さに水を充たし，水の中にはアルミニウムの細粉を浮游せしめて置く。

槽内の水には豫め鉛直の方向の溫度の傾を與へて置く。これは大氣の potential temperature が上に行く程高いことに相當する。而して，水槽の底の左半分の溫度を一定に保ち，右半分の溫度を徐々に上げると，底の冷溫の境界線の上に小さい循環流が出來，之が次第に發達して，左右兩方向へ擴がり，同時に流れの强さも增して行く。

Photo 1 から 7 までは，此の循環流の色々の狀態を示す。流れの向きは線から點の方に向いて居る。此等の寫眞は，原の寫眞の明瞭な線と點との全部を墨でなぞつてから燒附けたもので，2a と 3a とは 2 と 3 との原板である。

循還流は，底の溫められて居る側の先端の部分を除き，流線が殆んと完全な楕圓となる。Photo 1 は充分發達した循還流の中央部を示す。底の冷い側では，循還流の先端が來ると水は極めて徐々に運動を始め，其の速度を觀測し得る樣になれば，流線は楕圓形であることが分る。然るに，底の溫められて居る側では，循還流の到達する前に Photo 2 に示す樣な不規則な鉛直對流が發生する。楕圓循還流は，此等の不規則な對流による渦流を或は征服し或は併呑しつゝ進行ずる爲め，其の先端に明瞭な前線 (Front) を形成する。前線の前進する速度は，底の冷い側へ循還流の擴がる速度に比

べて遙に小さい。此の事は，循環流の發生後間も無く撮つた Photo 7 によつても明である。前線の狀態は Photo 3 及び 4 によつて見ることが出來る。

循環流々線の楕圓の長軸の位置に殆んど水平な無流層が出來る。循環流の高さを論ずるには，此の層の高さを考へるのが便利である。其の高さは循環流の發達と共に徐々に增加する。底の冷たい側では Photo 5 に示す樣に正しく水平な無流層が出來るが，底の溫められて居る側では Photo 6 に示す樣な渦流が發生する。

Photo 8 は循環流中央部の寫眞を，一秒づゝの間隔で一秒づゝ四回露出して撮つたものであつて，これによつて色々の高さの流速を測定することが出來る。其の結果を圖示したものが Fig. 2 である。無流層の高さの增す有樣も同圖によつて分る。

底面上 1 mm. の處へ極めて細い針金で作つた熱電對を置いて溫度を測つた結果が Fig. 3 と 4 とに示してある。Fig. 3 は色々の點に於ける溫度の上昇する狀態を示し，Fig. 4 は水槽の縱の方向の溫度分布を示す。

Fig. 5 は前線の位置を底の溫度不連續點から測つた距離を示すものであつて，線の傾きは前線の進む速度を與へる。

第二章　流體力學的計算

底の溫度の急變して居る點から測つた水平距離を x (底の溫い方を正とする)とし，底面から測つた高さを y とし，流體の深さを h とする。又平衡狀態に於ける (水槽實驗では底の半分を溫め初める前の) 各點の溫度 (大氣の場合には potential temperature) を Θ とし，α を流體の膨脹係數，流體の密度を ρ，流體の運動による壓力を p とすれば，加速ポテンシヤル ϖ/ρ は，本文第二章の (0) 式で表はされる。

流體が運動を初めた後の各點の溫度の Θ からの偏差を ϑ とし，ϑ 及び速度 u, v は小さいものと假定すれば，運動方程式 (1) 及び熱傳導の式 (2) が得られる。又，連續方程式は (3) である。此等の式に於て，β は溫度の鉛直方向の傾き (大氣の場合には potential temperature の傾き) 即ち $\partial\Theta/\partial y$ を表はし，γ は $g\alpha=\gamma$ と置いたもの，κ は溫度擴散率である。

限界條件は (4) の通りである。底面上に於ける溫度分布 $f(t, x)$ は實測の結果から定めなくてはならない。金屬製底面の溫度は勿論左右兩半に於ては一定で中央に於て急變して居るけれども，底面に極めて近い所の流體の溫度は，流體が x 方向に動いて居る爲め，溫度の不連續を有せず，第一章の Fig. 4 に示す樣になる。此の曲線は tanh で殆んど正確に表はすことが出來る。又，水槽實驗では底面を熱するに週期的に行はなかつたけれども，海陸風の場合を考へ，底面の右半を週期的に溫めたり冷したりしたと假定し，$f(t, x)$ を本文第二章 (6) の樣に置く。

斯くして，方程式を解くときは，流れの函數 ψ に對し (16)，溫度變化 ϑ に對し (17) の樣な解が得られる。

第三章　理論的解式の水槽實驗への應用

第一章に述べた水槽實驗の様に y/h が 1 に對して小さい場合には，(即ち循環流が水面に達せない場合には,) 解式 (16) を，本文第三章 ((3)) に示す様に簡約して用ひる事が出來る。

解式の含む定數 $\beta, \gamma, \sigma, C, b$ には實驗の際の狀態に適合する値を入れる。然るに，定數 κ は靜水の熱傳導による溫度分散率を用ひるのは勿論不適當であつて，此の場合には Photo 6 にある様な對流的原因による水の渦流が熱を鉛直方向に運ぶ事が溫度分散の殆んど全部であると考へてよい。而して，κ の値によつて，解式の與へる無流層の高さが大に變化するから，無流層の高さが理論と實驗と一致する様に κ の値を定めるのが最も適當と思はれる。水槽實驗の場合には $\kappa = 23{\cdot}8$ とすれば Fig. 2 に示す結果と無流層の高さが一致する。然るに，水の水平速度 $u = \partial\psi/\partial y$ は Fig. 2 の示す値よりも非常に大きくなる。此れは元の方程式に於て循環流に對する減衰力を省略してある結果であつて，實際の循環流は水の粘性によつて生ずる抵抗を不斷に受けつゝ發達したものであるから，其の强さは理論の示すものに或る係數 F を乘じたものである。此の係數 F を 0·062 とすれば，中央部に於ける流速は高さに對し Fig. 14 に示す様な變化をする。これは，底から 1·5 cm. ばかりの部分を除き，Fig. 2 と良く一致する。

理論に於ては底の加熱と冷却とは週期的に行ふものと假定したから，其の位相を與へる σt が 0, $\pi/4$, $\pi/2$, $3\pi/4$ なる場合の ψ の分布即ち流線の狀態を圖示すれば Fig. 15, 16, 17, 18 の様にる。$\sigma t = 0$ に於ては右半が冷却せられた間に出來た逆向きの循環流が存在する。$\sigma t = \pi/4$ では右半を溫めた爲めの循環流が下方に發生して居る。これが次第に發達して，$\pi/2$ と $3\pi/4$ との間で最大速度に達する。

Fig. 19 は x が 0, 10 cm., 20 cm. なる點に於ける最下層の流速の計算値の時と共に變る狀態を示す。$x = 0$ と $x = 10$ cm. との曲線が横軸を切る距離は 3° 即ち時間で 30 秒に相當するから，楕圓形循環流が中央から兩側に向つて擴がつて行く速度は 3·3 mm/sec. となる。底の冷い側では (正確な觀測は出來ないが) 此の速度は殆んど實際と一致して居る。然るに，底を溫めて居る側では，前線の進む速度は之よりも遙に小さい。これは，鉛直對流で充たされて居る所を楕圓循環流が無理に進んで行く爲めには，有限な dynamical pressure が必要な爲であると考へられる。第一章に述べた前線の進む速度 0·84 mm/sec. から見れば，前線に必要な dynamical pressure は流速 2·2 mm/sec. に相當するものと思はれる。

第四章　理論的解式の海陸風への應用

1930 年 7 月 15 日越中島海岸に於ける元の航空研究所で測風氣球による風速測定を行つた。當日は快晴で，傾度風は極めて小さかつた。Fig. 20 は午前 11 時午後 1 時及び 3 時に放つた氣球の每分後の位置と高さとを示す。Fig. 21 は Fig. 20 によつて

求めた各層の風速である。

當日の溫度記錄其の他から解式の含む定數を決定し，前章に於けると同樣，無風層の高さから溫度の鉛直方向の擴散率を求めると，$\kappa = 4{\cdot}5 \times 10^7$ となる。此の値は，大氣中の渦流によつて起る混合作用のみに因る κ の値を G. I. Taylor が求めたものよりも非常に大きいが，それは，前章にも述べた樣に，海風の循還流には鉛直對流による攪亂が伴つて居て，之が非常に大きな働きをなすから不思議はない。水槽實驗に於ても，右半を溫めたと同じ速度で冷やすときに生ずる循還流の無流層の高さは僅かに 1 cm. ばかりであつて，底を溫めた場合に比べて非常に小さな κ の値が出ることからでも明白である。

此の場合にも，循還流は粘性による抵抗を受けつゝ發達したものであるから，風速を求めるには $\partial\psi/\partial y$ に或る係數 F_1 を掛けなくてはならない。計算値と實測値とを比べて F_1 を求めると 0·1418 と出る。これを用ゐて午後 1 時に於ける海岸線上の各高さに對する風速を求めると，Fig. 21 に點線で引いた曲線の樣になる。之を實測曲線と比較して見ると，300 m. 以上ではよく一致して居ると云へる。300 m. 以下では實際の風は地表との摩擦によつて循還流に固有のものよりも小さくなつて居る。地上に於て，實測による風と計算によるものとの比 F_2 を求めると 0·448 であつて，地上風の傾度風に對する比よりも少し小さい。F_2 は地表の狀態によつて變化し，F_1 は循還流の發達と共に幾分變化するであらうけれども，此處には共に定數として議論を進める。

位相 σt が 0，$\pi/4$, $\pi/2$, $3\pi/4$ なるときの ψ の値の高さによる變化は Fig. 24 の樣になる。又，各層の風速 $(\partial\psi/\partial y)\times F_1$ は Fig. 25 に示す通りである。

海岸からの距離が 0，2 km., 5 km., 10 km., なる各點に於ける，計算地上風の時と共に變化する狀態を圖示すれば Fig. 26 の樣になる。海岸に於ける風速の變化を實測による値と比較して見ると，Fig. 28 に示す樣によく一致する。

陸地の上を海風の前線が進行する速度は，前線に於て必要とする dynamical pressure を (速度で表はして) 0，1 m/sec., 2 m/sec. と假定すれば Table IX に示す樣な値が得られる。其の結果から見て，前線の直ぐ後ろの風速は 1 m/sec. 附近であらうと思はれる。

No. 145.

(Published February 1937.)

Theoretical and Experimental Studies of Convectional Circulation and its Relation to Land and Sea-breezes[1]

By

Tatuo KOBAYASI, *Rigakuhakusi*,
Member of the Institute,

and

Tatudirô SASAKI, *Rigakuhakusi*,
Member of the Institute,

with the Assistance of

Tadao OSANAI, *Rigakusi*,
Laboratory Assistant.

Abstract.

The motion of the fluid developed when one half of its bottom was heated was solved mathematically, and the solution was compared with schematic experiments and also with observed data of sea breezes.

The schematic experiments were carried out with water in a tank. A vertical temperature gradient, which corresponds to the gradient of the potential temperature in the atmosphere, was given to the water. And then, the temperature of one half of the bottom of the tank was raised a few degrees. In this way, a circulation of elliptic paths was generated above the boundary of the warm and the cold halves. The velocities of the water and the speed of growth of the circulation were measured. The mathematical solution accords well with the results of the experiments, if a suitable value is given to the diffusibility of temperature in a verical direction, which the solution contains, and the effect of viscosity is taken into consideration.

In the case of sea breeze, the mathematical solution gives the relations of the rate of rising of the temperature on the earth's surface by the solar radiation to the wind velocities at various points and times, the height of the limit of the breeze and the speed of extension inland of the region covered by the breeze.

(1) A short account of this work was published in "Beiträge zur Physik der freien Atmosphäre, Bd. 19, (1932) (Bjerknes-Festschrift) S. 17."

I. Tank Experiments.

The tank used in the experiments, which was 300 cm. long and 20 cm. wide, was filled with water to a depth of 30 cm. The bottom of the tank was copper plate, which formed the upper sides of a pair of pipes of flat rectangular section, as shown in Fig. 1. (Not in correct proportion) Water of any temperature could be circulated through these pipes from small reservoirs by means of circulating pumps. In this way, each bottom half of the tank was heated or cooled to the desired temperature. In the experiments to be described, while the right half of the bottom was gradually heated or cooled, a constant temperature was

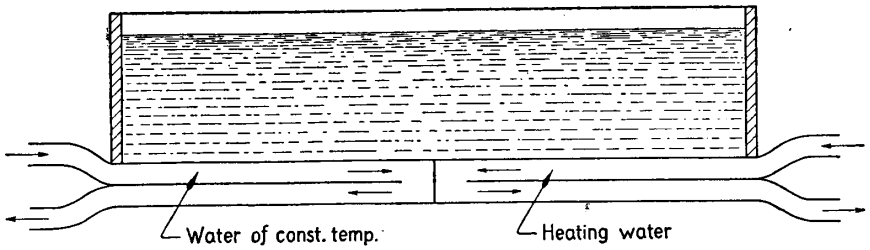

Fig. 1.

maintained in the left half. Very fine aluminium powder was dusted into the water in order to render its motion visible. The vertical section of the water about 1 cm. thick and parallel to the length of the tank at the middle of its breadth was illuminated from the upper surface of the water by a parallel beam of light from an arc lamp. The motion of the water was observed or photographed through the glass wall on the front side of the tank.

Before each experiment, a vertical temperature gradient of from 0·1° to 0·5° per cm. was imparted to the water. That the water temperature has a gradient corresponds to the fact that the potential temperature of the free atmosphere increases with height. Although the vertical temperature gradient does not alter the characteristic features relating to motion of the water, the greater the gradient the smaller the vertical scale of the fluid motion. If there were no temperature gradient

in the water, the circuratory motion would reach the upper surface of the water, whence it follows that the vertical gradient of the potential temperature in the atmosphere is the most important factor in limitting the height of a land or sea breeze.

After the vertical temperature gradient had been imparted to the water, the latter was allowed to stand for two or three hours until all movement of the water ceased.

The water in the reservoir was heated by an electric heater immersed in it. Two or three minutes after the heating had begun, a small (roughly circular) circulation started above the discontinuity of temperature at the bottom. At the same time, many small irregular vertical convection currents of 2 or 3 cm. height shot up from every part of the heated bottom. The circulation developed with time, much in horizontal scale, but little in vertical scale, so that it became elliptic. Photo 1 shows an elliptic circulation after it had fully developed.

In taking the photographs (Photo 1–7), the exposures lasted in all 5 seconds; exposed 3 seconds, interrupted 1 second and then exposed 1 second, so that each pair of a dot and dash gives the velocity of the fluid, the sense of motion being in direction from dash to dot.

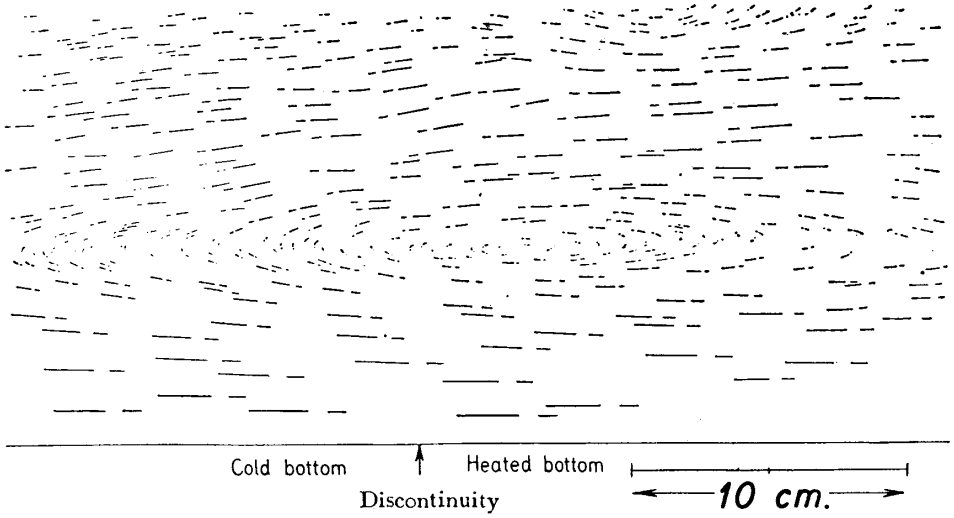

Photo 1.

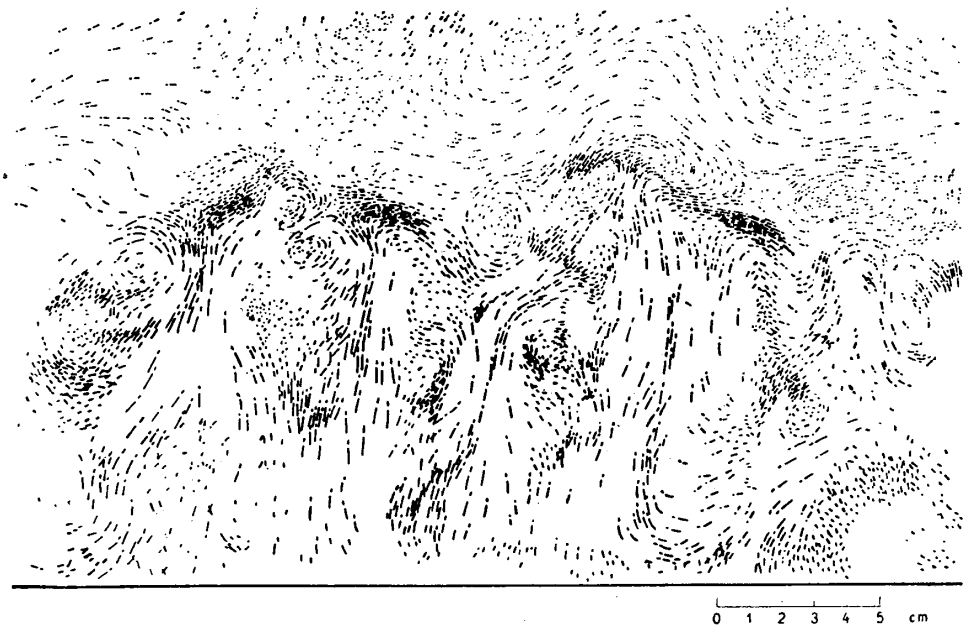

Photo 2.

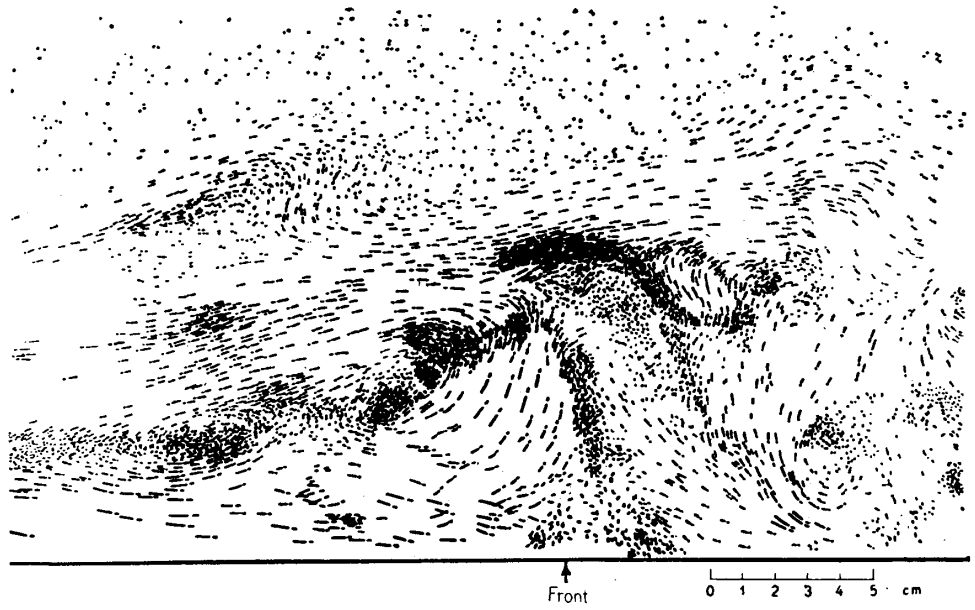

Photo 3.

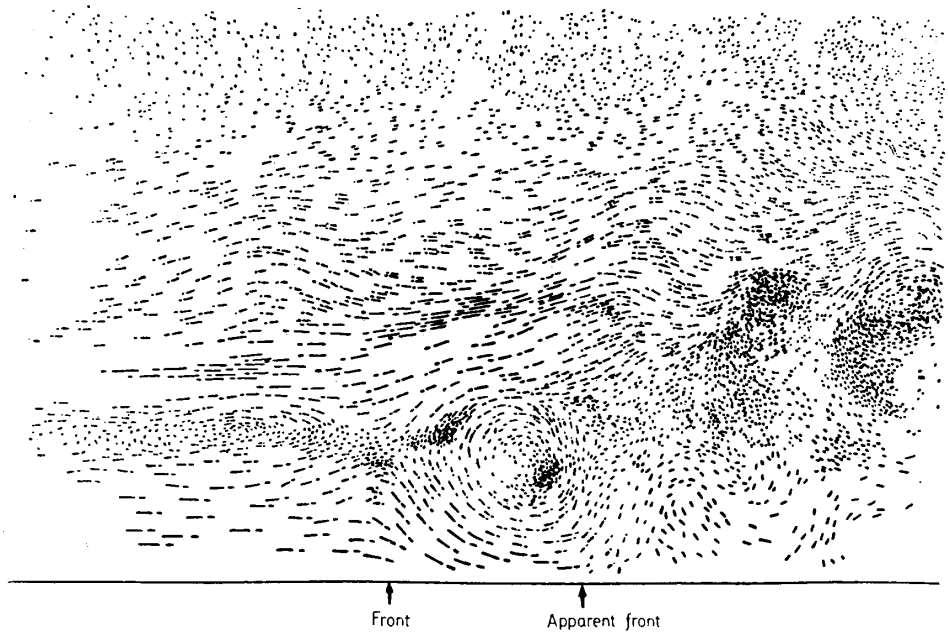

Photo 4.

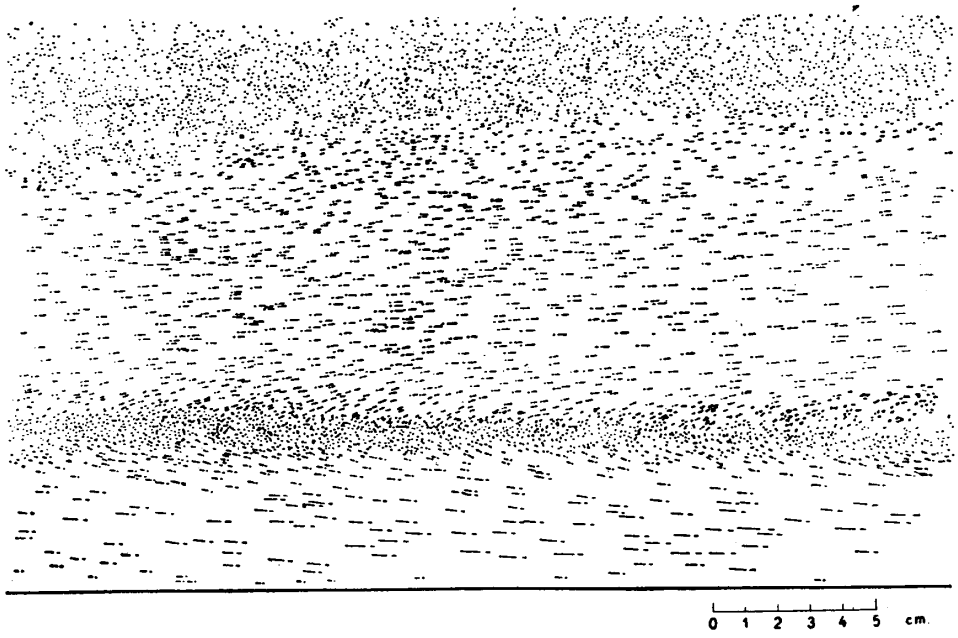

Photo 5.

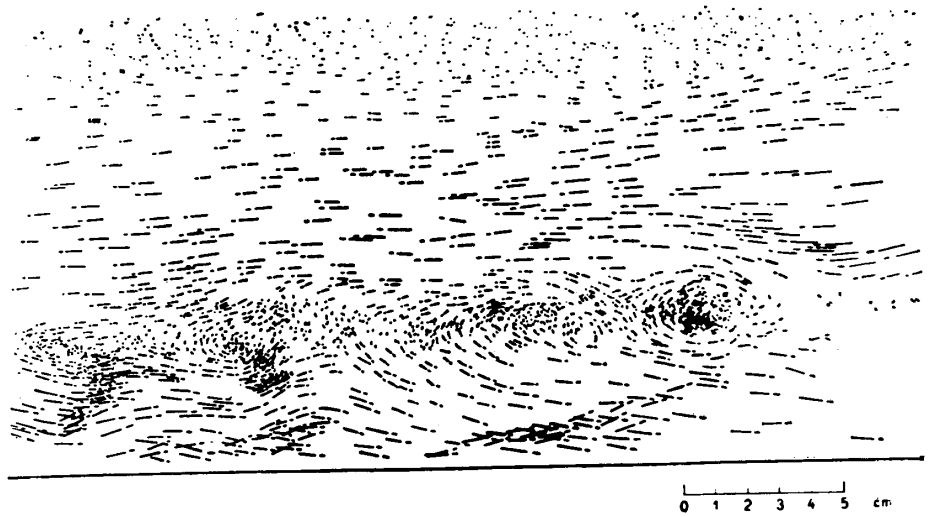

Photo 6.

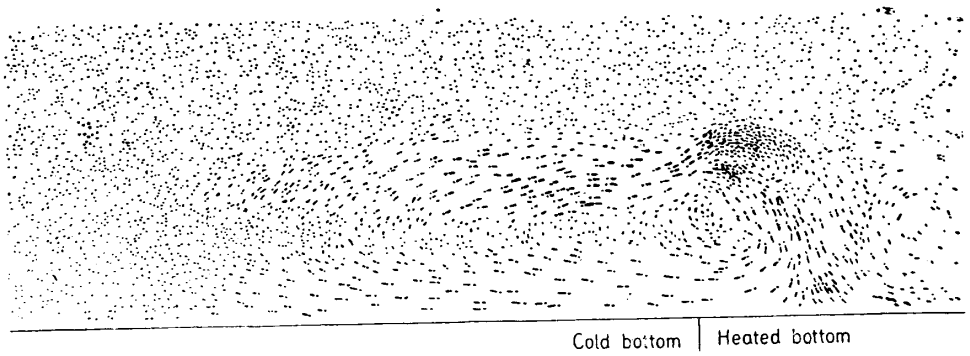

Photo 7.

Photos 1–7 were printed after tracing with ink all the distinct dots and dashes in the original photographs. Photos 2a and 3a are the respective originals of Photos 2 and 3.

The irregular vertical convections in the region of the heated half, where the ellipiic circulation had not yet reached, increased both in velocity and size, the neighbouring ones coalescing. Their tops had the exact form of cumulus clouds.

Photo 2 a.

Photo 3 a.

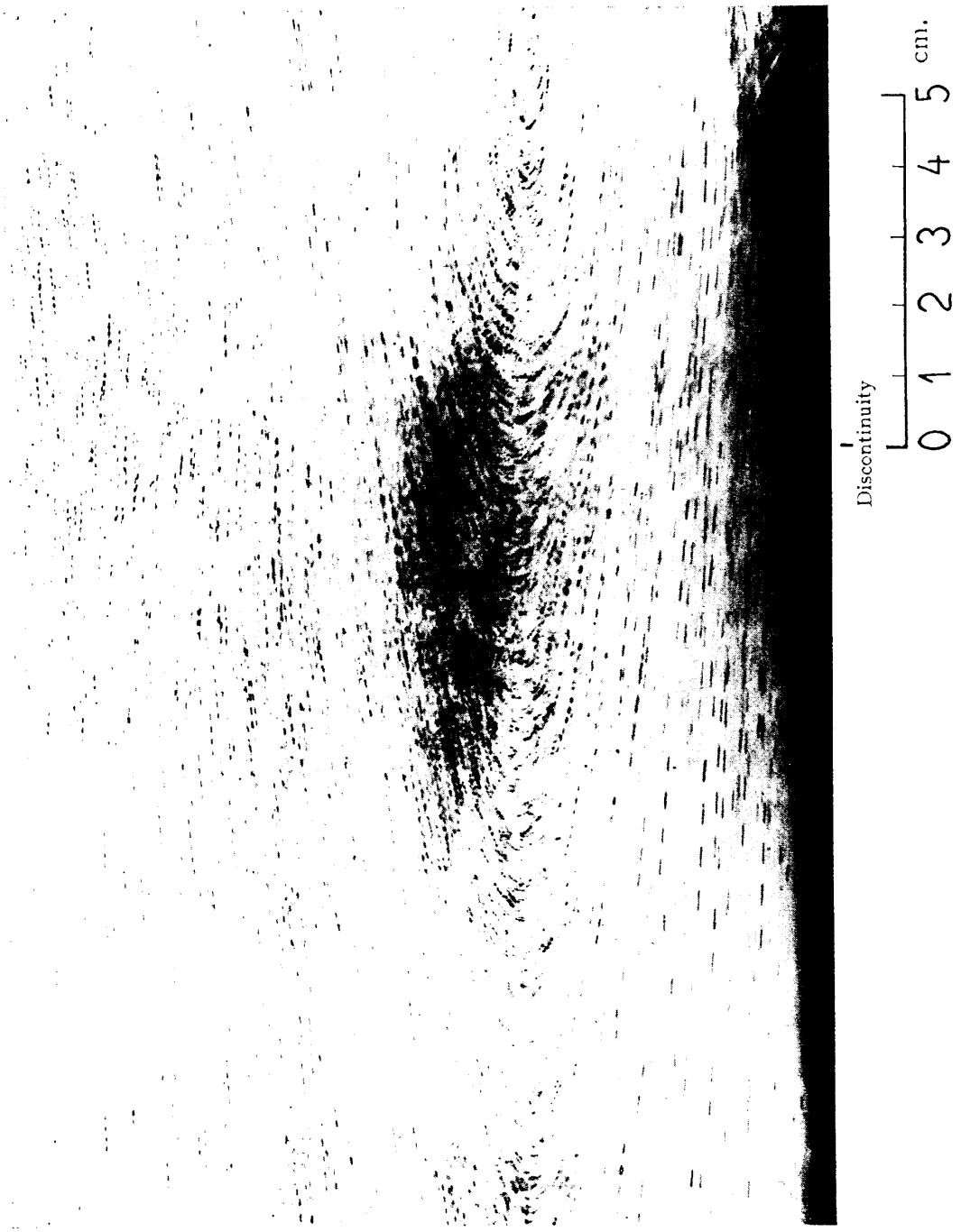

Photo 8.

The stream lines of the elliptic circulation in the cold half were very regular and perfectly elliptic, and the fluid began its motion so gradually upon arrival of the van part of the circulation that the exact limit of circulation could be defined only with difficulty. In contrast to this, the front of the circulation on the heated half of the bottom was very distinct, there being a steady horizontal flow in the region of elliptical circulation, while in the region of vertical convection the flows were very irregular, the vertical flows alone being conspicuous. The shape of the front differed with the extent to which a vortical flow of the same sense existing in the convectional region had been annexed. At one time its head rose high, as seen in Photo 3, while at another its head hung low in wedge form, as shown in Photo 4.

The elliptic circulation developed much more quickly towards the cold half than towards the heated half, as will be seen from Photo 7, which shows the circulation at an early stage of development. As the circulation grew towards the heated half, the stream lines showed more regular ellipses, as shown in Photo 1, and the center of the ellipses shifted gradually (a few centimeters at the end of the experiment) towards the heated half.

The elliptic circulation had a horizontal calm layer at the height of its major axis. Although this calm layer was always perfectly flat on the cold half of the bottom, as shown in Photo 5, on the heated bottom, especially when the heating was vigorous, many small vortical motions were produced along the calm layer, as will be seen from Photo 6.

The development of these elliptic circulations were examined quantitatively. In one of the experiments the initial temperature gradient in vertical direction was $0{\cdot}111^{\circ}$ per cm. and the rate of temperature rise of the heating water passing through the pipe below the bottom was $0{\cdot}33^{\circ}$ per minute. Three photographs of the central part of the circulation were taken at $6^{m}\ 45^{s}$, $10^{m}\ 30^{s}$ and $14^{m}\ 0^{s}$ after the heating was begun. One of those photographs is reproduced in Photo 8. In this case, four exposures of 1 second each were given with intervals of 1 second each.

The velocities of flow at different heights in the neighbourhood of the temperature discontinuity of the bottom were measured on those photographs.

The results are plotted in Fig. 2. The curves show the heights of the calm layers at respective times, which are 3·73 cm., 4·37 cm., and 5·05 cm. The curves bend sharply in the lowest 1–1·5 cm. and tend to zero at the bottom—evidently caused by resistance of the bottom due to viscosity of the fluid.

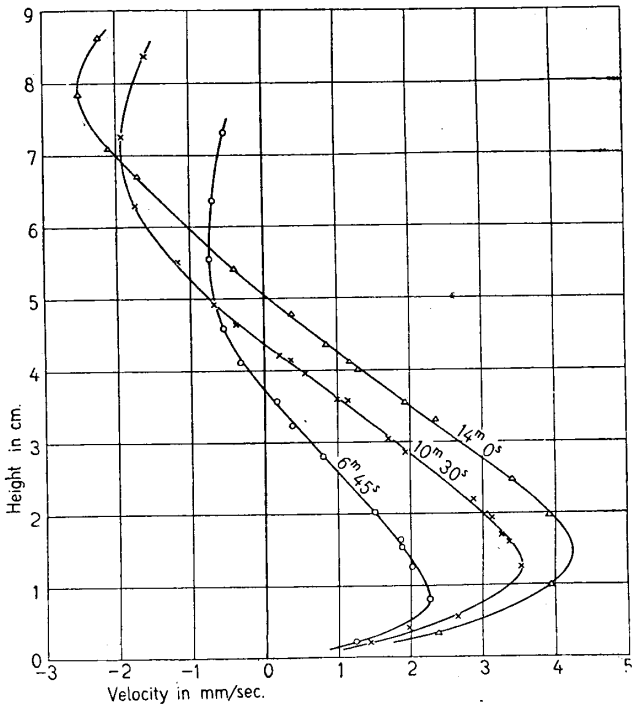

Fig. 2.

In order to measure the temperature of the water at different points and times, the experiments were repeated three times with conditions the same as just described. As it was very difficult to produce a uniform vertical temperature gradient of the required degree in the water, nonuniformities and inequalities to the extent of a few per cent. were unavoidable, the mean value of the gradient being 0·111 deg/cm. Thermo-

junctions made of very fine wires were held in support 1 mm. above the bottom at −15 cm., 0 cm., +15 cm., +30 cm., and +45 cm. towards the right from the discontinuity at the bottom, and the temperatures were measured a number of times in each experiment. As the temperatures indicated by the thermo-junctions fluctuated owing to vorticities in the flow, the results of the three experiments were plotted against the time by taking the intial temperatures as zero, as shown in Fig. 3, from which probable

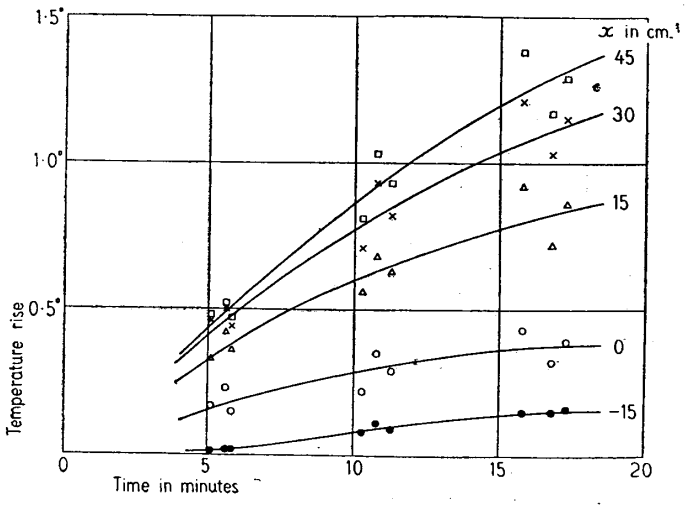

Fig. 3.

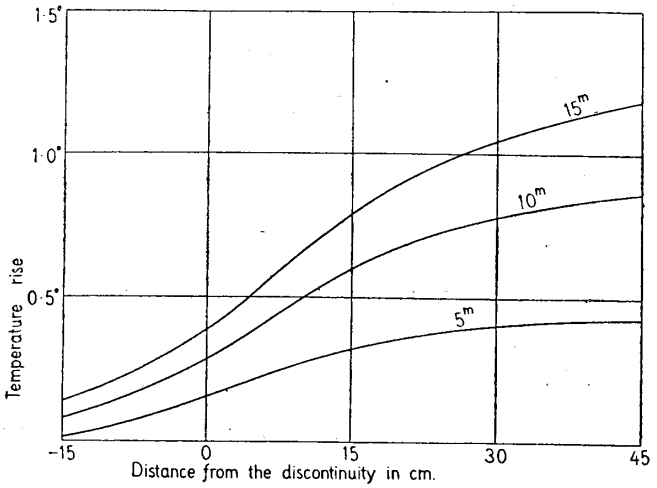

Fig. 4.

curves showing the temperature variations at those five points were drawn. Fig. 4, which was drawn from Fig. 3, shows the distributions of temperature in x direction at 5^m, 10^m, and 15^m after the heating had begun.

The positions of the circulation front were read off several times during each experiment and plotted against the time measured from the beginning of the heating, as shown in Fig. 5. The diagram shows that the circulation front started 2·4 minutes after the heating was begun and that its velocity of propagation was very nearly uniform, the value being 0·84 mm/sec.

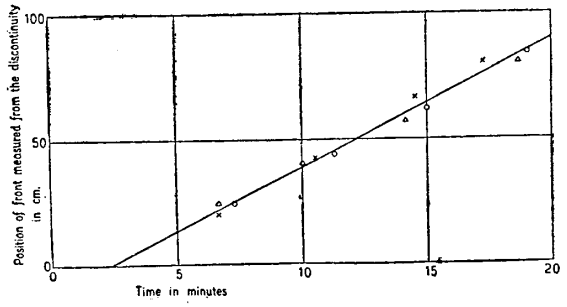

Fig. 5.

The cooling, instead of heating, of one half of the bottom produced a circulation of the reversed sense much flatter than in the case of heating, with the calm layer at 1–1·5 cm. height. The limits of the circulation on both halves of the bottom at any time were obscure, because the fluid began its motion very gradually.

II. Mathematical Investigation of Convectional Circulation.

Let x be the distance measured from the discontinuity at the bottom (the coast) and y the height measured from the bottom of the fluid. Let Θ be the temperature of the fluid at any point in the equilibrium state and ϑ the deviation of temperature from Θ at any time. As the variation in temperature is quite small in the persent problem, we may write

$$\rho = \rho_0 - \rho_0 \alpha \vartheta ,$$

where ρ is the density of the fluid, ρ_0 the same in the equilibrium state, and α the coefficient of expansion of the fluid.

Put $\partial\Theta/\partial y = \beta$; then β is the vertical gradient of initial temperature in the case of tank experiment and the vertical gradient of potential temperature in the equilibrium state in the case of land and sea breezes, and we may assume β to be a positive constant.

If the hydrodynamical pressure is denoted by p, the accelerational potential at any point in the fluid ϖ/ρ may be expressed thus:

$$\varpi = p + \rho g y - \rho g \alpha \int \Theta dy \,. \qquad (0)$$

If we assume that the components of velocity u, v, and the disturbance of the temperature ϑ are small, the equations of the fluid motion and the heat conduction reduce to

$$\frac{\partial u}{\partial t} = -\frac{1}{\rho_0}\frac{\partial \varpi}{\partial x}, \quad \frac{\partial v}{\partial t} = -\frac{1}{\rho_0}\frac{\partial \varpi}{\partial y} + \gamma\vartheta, \qquad (1)$$

$$\frac{\partial \vartheta}{\partial t} + \beta v = \kappa\left(\frac{\partial^2 \vartheta}{\partial x^2} + \frac{\partial^2 \vartheta}{\partial y^2}\right), \qquad (2)$$

and the equation of continuity is

$$\frac{\partial u}{\partial x} + \frac{\partial v}{\partial y} = 0, \qquad (3)$$

where $\gamma = g\alpha$, and κ stands for the diffusibility of temperature. We will assume that the effect of pressure on the density of the fluid may be neglected even in the case of land and sea breezes, and that ρ_0 is constant. (Boussinesq has shown that this assumption is regitimate[1]).

The boundary conditions to be satisfied are

$$\left.\begin{aligned} v = 0 \quad &\text{and} \quad \vartheta = 0 \qquad \text{at} \quad y = h, \\ v = 0 \quad &\text{and} \quad \vartheta = f(t, x) \quad \text{at} \quad y = 0, \end{aligned}\right\} \qquad (4)$$

(1) Boussinesq: Théorie Analytique de la Chaleur. t. II, p. 172, (1903). See also "Lord Rayleigh: Scientific Papers, Vol. VI, p. 436."

where $f(t, x)$ is the function which represents the temperature distribution on the bottom, and h the height of the limit of the fluid which takes part in the fluid motion considered.

If we introduce the stream function ψ such as

$$u = \frac{\partial \psi}{\partial y}, \quad v = -\frac{\partial \psi}{\partial x},$$

we get the differential equation for ψ from (1), (2) and (3) as follows:

$$\frac{\partial^2}{\partial t^2}\nabla^2\psi - \kappa\frac{\partial}{\partial t}\nabla^4\psi + \beta\gamma\frac{\partial^2\psi}{\partial x^2} = 0. \qquad (5)$$

In order to get the solution of this differential equation, put

$$\psi = e^{i\sigma t}\sin ax\, F(y),$$

then, we get from (5)

$$F(y) = A\frac{\sinh c_1(y-h)}{\sin c_1 h} - B\frac{\sinh c_2(y-h)}{\sinh c_2 h},$$

where

$$c_1^2 = a^2 - \frac{\sigma^2 + \sqrt{\sigma^4 - 4i\kappa\sigma\beta\gamma a^2}}{2i\kappa\sigma},$$

$$c_2^2 = a^2 - \frac{\sigma^2 - \sqrt{\sigma^4 - 4i\kappa\sigma\beta\gamma a^2}}{2i\kappa\sigma}.$$

In the tank experiment, the temperature of the metal bottom is uniform in each half and has a jump at the boundary of both halves. However, the temperature of the fluid just above the bottom shows no discontinuity and have such distribution as shown in Fig. 4, owing to the horizontal motion of the fluid. On the heating of the bottom, we will assume, taking the case of land and sea breezes into account, that the heating and cooling were done periodically. Then we may choose a form of function as shown below for $f(t, x)$ in the boundary conditions (4):

$$f(t, x) = \frac{C}{2} \sin \sigma t \left[\tanh \frac{bx}{2} + 1 \right]. \tag{6}$$

Now, since

$$\frac{1}{2}\left[\tanh \frac{bx}{2} + 1 \right] = \frac{1}{1+e^{-bx}} = \frac{1}{\pi} \int_0^\infty \int_{-\infty}^\infty \frac{\cos a(x-\lambda)}{1+e^{-b\lambda}} da d\lambda ,$$

if we put as the appropriate solution of (5)

$$\Psi = -iC\kappa\gamma e^{i\sigma t} \frac{1}{\pi} \int_0^\infty \int_{-\infty}^\infty \frac{a \sin a(x-\lambda)}{1+e^{-b\lambda}} \cdot \frac{1}{\sqrt{\sigma^4 - 4i\kappa\sigma\beta\gamma a^2}}$$

$$\times \left\{ \frac{\sinh c_1(y-h)}{\sinh c_1 h} - \frac{\sinh c_2(y-h)}{\sinh c_2 h} \right\} da d\lambda , \tag{7}$$

we get

$$\theta = -\frac{1}{\gamma} \frac{\partial}{\partial t} \int \nabla^2 \Psi dx = \frac{C\kappa\sigma}{\pi} e^{i\sigma t} \int_0^\infty \int_{-\infty}^\infty \frac{\cos a(x-\lambda)}{1+e^{-b\lambda}}$$

$$\times \frac{1}{\sqrt{\sigma^4 - 4i\kappa\sigma\beta\gamma a^2}} \left\{ (c_1^2 - a^2) \frac{\sinh c_1(y-h)}{\sinh c_1 h} \right.$$

$$\left. - (c_2^2 - a^2) \frac{\sinh c_2(y-h)}{\sinh c_2 h} \right\} da d\lambda \tag{8}$$

From this equation we see that $\theta = 0$ at $y = h$, and

$$\theta_{y=0} = -iCe^{i\sigma t} \frac{1}{\pi} \int_0^\infty \int_{-\infty}^\infty \frac{\cos a(x-\lambda)}{1+e^{-b\lambda}} da d\lambda$$

$$= -i\frac{C}{2} e^{i\sigma t} \left[\tanh \frac{bx}{2} + 1 \right]$$

at $y = 0$. Hence, if we denote the real part of θ by ϑ, we get

$$\vartheta_{y=0} = \frac{C}{2} \sin \sigma t \left[\tanh \frac{bx}{2} + 1 \right]$$

which is the condition (6).

As the expression for Ψ in (7) and that for θ in (8) contain $e^{i\sigma t}$ as a factor, we get

$$\theta = -\frac{1}{\gamma} i\sigma \int F^2 \Psi dx$$

It is evident from this equation that $-\Im(\Psi)$ corresponds to $\Re(\theta)$. Hence, if we choose ϑ as the real part of θ, the stream function ψ is to be chosen as the imaginary part of Ψ with negative sign before it. We can easily prove from (7) that $v = 0$ at $y = 0$ and $y = h$.

From the foregoing considerations we see that $-\Im(\Psi)$ and $\Re(\theta)$ are the required solutions of the differential equations (1), (2) and (3).

Next, we must carry out the integrations which appear in the solutions above.

In the rectangular region as shown in Fig. 6, we perform the contour integral

$$\int \frac{e^{iaz} dz}{1 + e^{-bx}} .$$

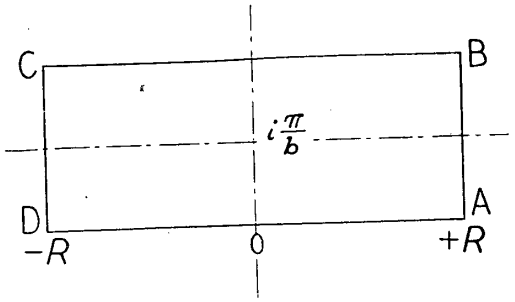

Fig. 6.

This integral reduces to

$$\int_{-R}^{R} \frac{e^{iax} dx}{1 + e^{-bx}}$$

on the real axis, and to

$$\int_{-R+i\frac{2\pi}{b}}^{R+i\frac{2\pi}{b}} \frac{e^{iaz} dz}{1 + e^{-bz}} = \int_{-R}^{R} \frac{e^{iax} e^{-\frac{2a\pi}{b}} dx}{1 + e^{-bx}}$$

on the line parallel to the real axis at a distance of $i\frac{2\pi}{b}$.

On AB

$$\int_{R}^{R+i\frac{2\pi}{b}} \frac{e^{iaz}}{1 + e^{-bz}} dz = \int_{0}^{\frac{2\pi}{b}} \frac{e^{ia(R+iy)} i dy}{1 + e^{-b(R+iy)}}$$

$$= ie^{iaR} \int_{0}^{\frac{2\pi}{b}} \frac{e^{-ay} dy}{1 + e^{-bR} e^{-iby}} .$$

When R tends to infinity,

$$\lim_{R\to\infty}\int_0^{\frac{2\pi}{b}}\frac{e^{-ay}dy}{1+e^{-bR}e^{-iby}}=\int_0^{\frac{2\pi}{b}}e^{-ay}dy=\frac{1}{a}\left[1-e^{-\frac{2\pi a}{b}}\right].$$

Similarly

$$\lim_{R\to\infty}\int_{-R}^{-R+i\frac{2\pi}{b}}\frac{e^{iaz}dz}{1+e^{-bz}}=i\lim_{R\to\infty}\int_0^{\frac{2\pi}{b}}\frac{e^{-iaR}e^{-ay}dy}{1+e^{bR}e^{-iby}}=0.$$

Hence, the integral on DC tends to 0 as R tends to infinity.

Therefore, when $R\to\infty$,

$$\oint\frac{e^{iaz}dz}{1+e^{-bz}}=\left(1-e^{-\frac{2a\pi}{b}}\right)\int_{-\infty}^{\infty}\frac{e^{iax}dx}{1+e^{-bx}}+\frac{ie^{iaR}}{a}\left(1-e^{-\frac{2\pi a}{b}}\right)$$

$$=2\pi i\operatorname*{Res}_{z=i\frac{\pi}{b}}\left(\frac{e^{iaz}}{1+e^{-bz}}\right)=2\pi i\frac{e^{-\frac{a\pi}{b}}}{b}.$$

Hence

$$\int_{-\infty}^{\infty}\frac{e^{iax}dx}{1+e^{-bx}}=-\frac{ie^{iaR}}{a}+\frac{\pi i}{b}\frac{1}{\sinh\frac{\pi a}{b}}.$$

Using this result, we get

$$\int_0^{\infty}\int_{-\infty}^{\infty}\frac{a\sin a(x-\lambda)da\,d\lambda}{1+e^{-b\lambda}}$$

$$=\int_0^{\infty}\int_{-\infty}^{\infty}\frac{a\sin ax\cos a\lambda\,da\,d\lambda}{1+e^{-b\lambda}}-\int_0^{\infty}\int_{-\infty}^{\infty}\frac{a\cos ax\sin a\lambda\,da\,d\lambda}{1+e^{-b\lambda}}$$

$$=-\int_0^{\infty}a\cos ax\left(-\frac{\cos aR}{a}+\frac{\pi}{b\sinh\frac{\pi a}{b}}\right)da+\int_0^{\infty}\frac{a\sin ax\sin aR}{a}da$$

$$=\int_0^{\infty}\cos a(R-x)da-\int_0^{\infty}\frac{a\pi\cos ax}{b\sinh\frac{\pi a}{b}}da.$$

Also, we get

$$\int_0^\infty \int_{-\infty}^\infty \frac{\cos a(x-\lambda)}{1+e^{-b\lambda}} da\, d\lambda = \int_0^\infty \frac{\cos ax \sin aR}{a} da + \int_0^\infty \frac{\pi \sin ax\, da}{b \sinh \frac{\pi a}{b}}$$

$$-\int_0^\infty \frac{\sin ax \cos aR}{a} da = \int_0^\infty \frac{\sin a(R-x) da}{a} + \int_0^\infty \frac{\pi \sin ax\, da}{b \sinh \frac{\pi a}{b}} .$$

As shown above, if we perform the integration with respect to λ, the expressions for ψ and ϑ reduce from (7) and (8) to

$$\psi = \Im i C_{\kappa\gamma} \frac{e^{i\sigma t}}{\pi} \left\{ \int_0^\infty \frac{\cos a(R-x)}{\sqrt{\sigma^4 - 4i\kappa\sigma\beta\gamma a^2}} \left[\frac{\sinh c_1(y-h)}{\sinh c_2 h} - \frac{\sinh c_2(y-h)}{\sin c_2 h} \right] da \right.$$

$$\left. - \int_0^\infty \frac{a\pi \cos ax}{b \sinh \frac{\pi a}{b}} \frac{1}{\sqrt{\sigma^4 - 4i\kappa\sigma\beta\gamma a^2}} \left[\frac{\sin c_1(y-h)}{\sin c_1 h} - \frac{\sin c_2(y-h)}{\sinh c_2 h} \right] da \right. \tag{9}$$

$$\vartheta = \Re \frac{C_{\kappa\sigma}}{\pi} e^{i\sigma t} \left\{ \int_0^\infty \frac{\sin a(R-x)}{a\sqrt{\sigma^4 - 4i\kappa\sigma\beta\gamma a^2}} \right.$$

$$\times \left[(c_1^2 - a^2) \frac{\sinh c_1(y-h)}{\sinh c_1 h} - (c_2 - a) \frac{\sinh c_2(y-h)}{\sinh c_2 h} \right] da$$

$$+ \int_0^\infty \frac{\pi \sin ax}{b \sinh \frac{\pi a}{b} \sqrt{\sigma^4 - 4i\kappa\sigma\beta\gamma a^2}}$$

$$\left. \times \left[(c_1^2 - a^2) \frac{\sinh c_1(y-h)}{\sinh c_1 h} - (c_2^2 - a^2) \frac{\sinh c_2(y-h)}{\sinh c_2 h} \right] da \right\} . \tag{10}$$

[I] We first perform the integration

$$\int_0^\infty \frac{a \cos a\xi}{\sinh \frac{\pi a}{b}} \left\{ \frac{\sinh c_1 \eta}{\sinh c_1 h} - \frac{\sinh c_2 \eta}{\sinh c_2 h} \right\} \frac{da}{\sqrt{\sigma^4 - 4i\kappa\sigma\beta\gamma a^2}} , \tag{11}$$

which appears in the expression for ψ.

Put

$$I = \sigma^4 - 4i\kappa\sigma\beta\gamma a^2 ,$$

$$a = e^{-i\frac{\pi}{4}} \frac{\sigma^2}{2\sqrt{\kappa\sigma\beta\gamma}} z ,$$

then we get

$$I = \sigma^4(1-z^2) ,$$

$$c_1^2 = a^2 - \frac{\sigma^2 + \sqrt{\sigma^4 - 4i\kappa\sigma\beta\gamma a^2}}{2i\kappa\sigma}$$

$$= -i\frac{\sigma^4}{4\kappa\sigma\beta\gamma}\left[z^2 - \frac{2\beta\gamma}{\sigma^2}(1+\sqrt{1-z^2})\right].$$

If we further put

$$c_1 = e^{-i\frac{\pi}{4}} \frac{\sigma^2}{2\sqrt{\kappa\sigma\beta\gamma}} \zeta ,$$

we get

$$\zeta^2 = z^2 - \frac{2\beta\gamma}{\sigma^2}(1+\sqrt{1-z^2})$$

$$= -\left(\sqrt{1-z^2} - 1 + \frac{2\beta\gamma}{\sigma^2}\right)(\sqrt{1-z^2}+1)$$

Let the points corresponding to the roots of the equations

$$\sqrt{1-z^2}+1 = 0 \quad \text{and} \quad \sqrt{1-z^2} - 1 + \frac{2\beta\gamma}{\sigma^2} = 0$$

be z_1 and z_2 respectively.

Now transform t-plane into z-plane by the relation $t = \sqrt{1-z^2}$. Then the whole t-plane is represented conformally into the two sheeted Riemann surface in the z-plane, with $z = 1$ and $z = -1$ as its branch points. On the upper sheet of the Riemann surface, the point $z = 0$ corresponds

to $t = 1$, and the point corresponding to z_2 lies on the negative y-axis, because, as it is clear from the following numerical calculations, $2\beta\gamma/\sigma$ takes a value greater than 1. Similarly, on the lower sheet of the Riemann surface, $z = 0$ corresponds to z_1, and z_2 lies on the positive y-axis.

Let X and Y be the absolute values of the real part and the imaginary part respectively of the variable t, then the value of t on the two sheeted Riemann surface in the z-plane is shown in Fig. 7.

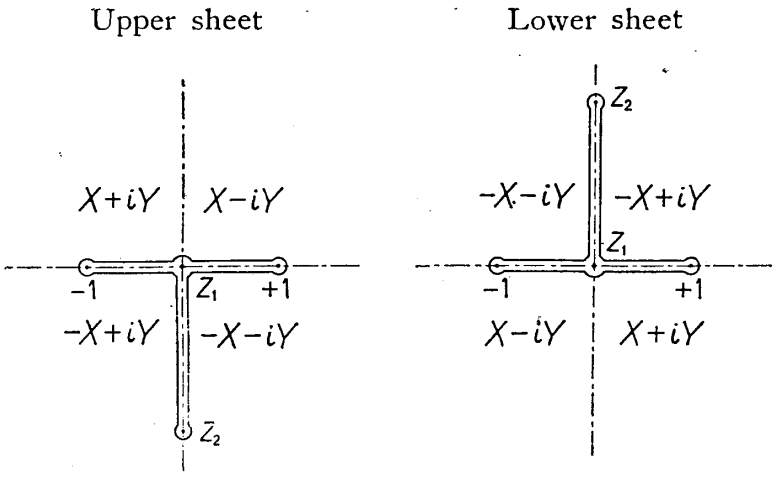

Fig. 7.

The whole ζ-plane is represented conformally into the four sheeted Riemann surface in the z-plane, with $z = -1$, $z = 1$, $z = z_1$ and $z = z_2$ as its branch points. The slit between $z = -1$ and $z = 1$ connects the first sheet to the third sheet, and the slit between $z = z_1$ and $z = z_2$ connects the first sheet to the second sheet and the third sheet to the fourth sheet. Every sheet of the Riemann surface in the z-plane is shown in Fig. 8.

The values $c_1 = \pm\frac{n\pi}{ih}$ satisfy the equation $\sinh c_1 h = 0$; and seeing that $c_1 = e^{-i\frac{\pi}{4}}\frac{\sigma^2}{2\sqrt{\kappa\sigma\beta\gamma}}\zeta$, we may write

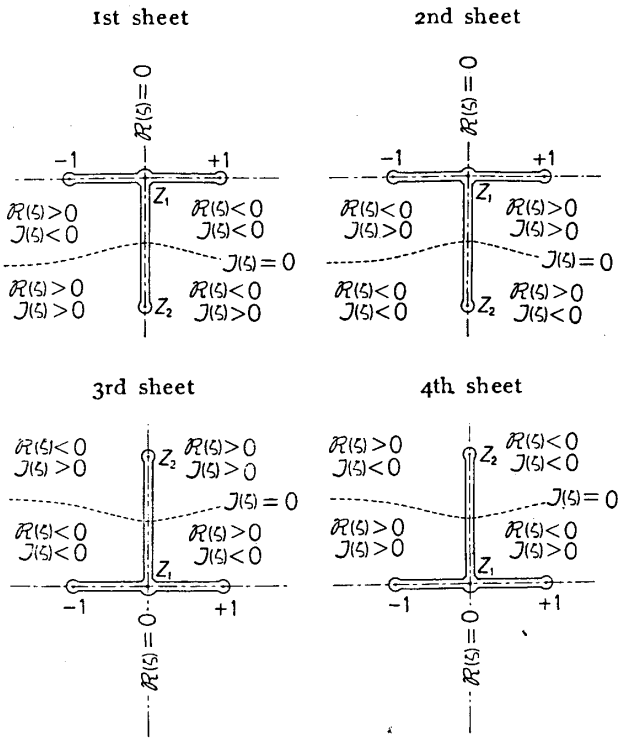

Fig. 8.

$$\zeta = \pm \frac{n\pi}{ih} \frac{2\sqrt{\kappa\sigma\beta\gamma}}{\sigma^2} e^{i\frac{\pi}{4}} = \pm \frac{n\pi}{h} \frac{2\sqrt{\kappa\sigma\beta\gamma}}{\sigma^2} e^{-i\frac{\pi}{4}}$$

$$= \pm nMe^{-i\frac{\pi}{4}} \text{ (say)}$$

as the values which satisfy the equation $\sinh c_1 h = 0$.

Since we can write $\zeta = \sqrt{-\left(t+\frac{\beta\gamma}{\sigma}\right)^2+\left(\frac{\beta\gamma}{\sigma}-1\right)^2}$, we may put

$$\zeta = \sqrt{A^2-t'^2},$$

where $A = \frac{\beta\gamma}{\sigma}-1$ and $t' = t+\frac{\beta\gamma}{\sigma}$.

Therefore at $\zeta = \pm nMe^{-i\frac{\pi}{4}}$, where the equation $\sinh c_1 h = 0$ is satisfied,

$$t'^2 = A^2 + in^2M^2 .$$

The points in the t'-plane corresponding to the roots of this equation are shown by marks ⊙ in Fig. 9.

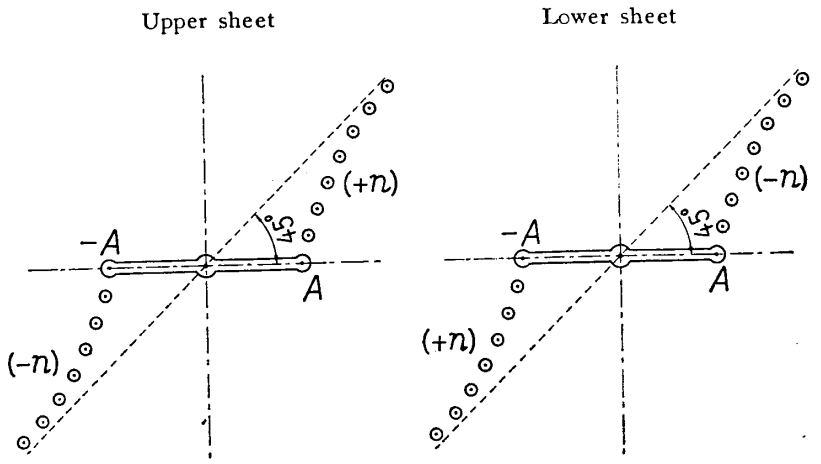

Fig. 9. t'-plane

The positions of these points on the first and third sheets of the four sheeted Riemann surface in the z-plane are shown by the same marks in Fig. 10.

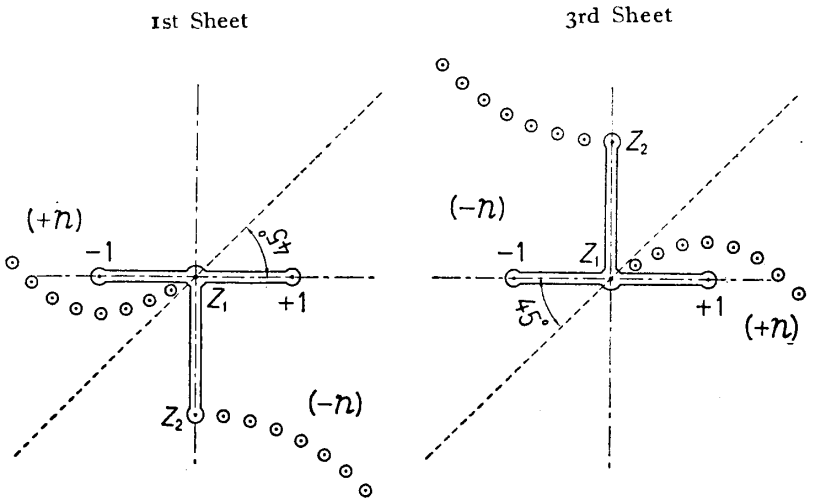

Fig. 10.

If we put $A_0 = \frac{\sigma^2}{2\sqrt{\kappa\sigma\beta\gamma}} e^{-i\frac{\pi}{4}}$, $B = \frac{2\beta\gamma}{\sigma^2}$ and $A_1 = \frac{\pi}{b} A_0$,

we may write

$$I = \int \frac{A_0 z e^{iA_0 z^2}}{\sinh A_1 z \sqrt{1-z^2}} \times \frac{\sinh A_0 \sqrt{z^2 - B(1+\sqrt{1-z^2})}\eta}{\sinh A_0 \sqrt{z^2 - B(1+\sqrt{1-z^2})}h} dz .$$

We now perform this integration on the Riemann surface. We take the contour **PABA′CP** (**P** and **C** are at an infinite distance from **A** or **A′**) as shown in Fig. 11 on the first sheet of the Riemann surface. This contour integral is divided as follows:

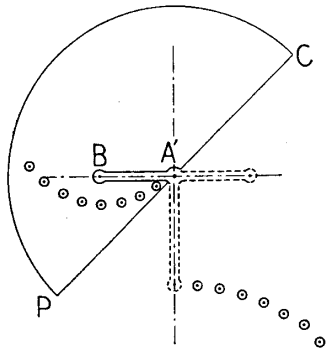

Fig. 11.

(1) On **A′C**, $z = re^{i\frac{\pi}{4}}$, hence

$$I_{A'C} = \int_0^\infty \frac{A_0 r e^{i\frac{\pi}{4}} e^{iA_0 e^{i\frac{\pi}{4}} r^2}}{\sinh r e^{i\frac{\pi}{4}} A_1 \cdot \sqrt{1-ir^2}} \times \frac{\sinh A_0 \sqrt{ir^2 - B(1+\sqrt{1-ir^2})}\eta}{\sinh A_0 \sqrt{ir^2 - B(1+\sqrt{1-ir^2})}h} e^{i\frac{\pi}{4}} dr .$$

(2) On **PA**, $z = re^{i\left(\frac{\pi}{4}+\pi\right)}$ and $\sqrt{1-ir^2}$ takes negative sign, hence

$$I_{PA} = -\int_0^\infty \frac{A_0 r e^{i\frac{\pi}{4}} e^{-iA_0 e^{i\frac{\pi}{4}} r^2}}{\sinh r e^{i\frac{\pi}{4}} A_1 \cdot \sqrt{1-ir^2}} \times \frac{\sinh A_0 \sqrt{ir^2 - B(1-\sqrt{1-ir^2})}\eta}{\sinh A_0 \sqrt{ir^2 - B(1-\sqrt{1-ir^2})}h} e^{i\frac{\pi}{4}} dr .$$

(3) On **AB**, $z = -x$ and $\sqrt{1-z^2} = \sqrt{1-x^2}$, hence

$$I_{AB} = -\int_C^1 \frac{A_0 x e^{-iA_0 x}}{\sinh A_1 x \sqrt{1-x^2}} \times \frac{\sinh A_0 \sqrt{x^2 - B(1+\sqrt{1-x^2})}\eta}{\sinh A_0 \sqrt{x^2 - B(1+\sqrt{1-x^2})}h} dx .$$

(4) On **BA′**, $z = -x$ and $\sqrt{1-z^2} = -\sqrt{1-x^2}$, hence

$$I_{BA'} = -\int_0^1 \frac{A_0 x e^{-iA_0 x^2}}{\sinh A_1 x \cdot \sqrt{1-x^2}} \times \frac{\sinh A_0 \sqrt{x^2 - B(1-\sqrt{1-x^2})}\eta}{\sinh A_0 \sqrt{x^2 - B(1-\sqrt{1-x^2})}h} dx .$$

(5) Consider a circle, A as its center, where $t=-1$. Let $t+1=t'$, and put $t'=\tau^2$, then

$$\zeta=\sqrt{-\left(t'-2+\frac{2\beta\gamma}{\sigma^2}\right)t'}=\sqrt{-\left(\tau^2-2+\frac{2\beta\gamma}{\sigma^2}\right)}\cdot\tau,$$

and

$$z=\sqrt{1-t^2}=\sqrt{1-(t'-1)^2}=\sqrt{2\tau^2-\tau^4}=\tau\sqrt{2-\tau^2},$$

hence

$$dz=\frac{2(1-\tau^2)}{\sqrt{2-\tau^2}}d\tau.$$

Therefore, if we carry out the integration in the τ-plane, we get

$$I=\int\frac{A_0\tau\sqrt{2-\tau^2}e^{iA_0\xi\tau\sqrt{2-\tau^2}}}{\sinh\tau\sqrt{2-\tau^2}A_1\cdot(1-\tau^2)}\times\frac{\sinh A_0\sqrt{2-\frac{2\beta\gamma}{\sigma^2}-\tau^2}\cdot\tau\eta}{\sinh A_0\sqrt{2-\frac{2\beta\gamma}{\sigma^2}-\tau^2}\cdot\tau h}\times\frac{2(1-\tau^2)d\tau}{\sqrt{2-\tau^2}}$$

$$=\int Pd\tau. \quad \text{(say)}$$

Since

$$\lim_{\tau\to0}\tau P=\lim_{\tau\to0}\left[+\sqrt{2}\frac{A_0}{A_1}\cdot\frac{\eta}{h}\cdot\tau\right]=0,$$

A is not a pole of the function P. Hence we get

$$I=0.$$

(6) Consider a circle, B as its center, where $z=-1$ and $\zeta=\sqrt{1-B}$. Put $z+1=\tau^2$, then $\sqrt{1-z^2}=\sqrt{2-\tau^2}\tau$, hence $dz=2\tau\,d\tau$. If we carry out the integration in the τ-plane, we get

$$I=\int\frac{A_0(\tau^2-1)}{\sinh(\tau^2-1)A_1}\times\frac{e^{-iA_0\xi}}{\tau\sqrt{2-\tau^2}}\times\frac{\sinh A_0\sqrt{1-B}\eta}{\sinh A_0\sqrt{1-B}h}\times2\tau d\tau=\int Qd\tau \text{ (say)}.$$

Since

$$\lim_{\tau\to0}\tau Q=0,$$

$z=-1$ is not a pole of the function Q. Hence we get

$$I=0.$$

(7) We next carry out the integration along the semi-circle of infinite redius. Let $z=\frac{1}{z'}$, then

$$\zeta=\frac{\sqrt{1-Bz'(1+\sqrt{z'^2-1})}}{z'}.$$

Hence, if z' is taken very close to 0, the integral can be written as follows:

$$I_{CP}=-\int \frac{e^{i\frac{A_0\xi}{z'}}}{i}\times\frac{\sinh\frac{A_0\eta}{z'}}{\sinh\frac{A_0h}{z'}}\times\frac{A_0}{\sinh\frac{A_1}{z'}}\times\frac{dz'}{z'^2}.$$

Seeing that

$$\lim_{z\to 0}\frac{\sinh\frac{A_0\eta}{z'}}{\sinh\frac{A_0h}{z'}}=\lim_{n\to\infty}\left(\frac{\eta}{h}\right)^{2n+1}=\begin{cases}0, & \text{when } \eta<h,\\ 1, & \text{when } \eta=h,\end{cases}$$

and

$$\lim_{z'\to 0}\frac{1}{z'\sinh\frac{A_0}{z'}}=\lim_{R\to\infty}\frac{Re^{i\theta}}{\sinh(RA_0e^{i\theta})}=\lim_{R\to\infty}\frac{1}{A_0\cosh(RA_0e^{i\theta})}=0,$$

except at $\theta=\frac{\pi}{2}+\frac{\pi}{4}$, when it is indeterminate, but not infinity, we have to consider the integral $\int\frac{e^{iA_0\xi z}}{z}dz$ in order to carry out the integration of I_{CP}.

There are two cases,

(a) $\xi\geqq 0$ and (b) $\xi\leqq 0$.

(a) The case where $\xi \geqq 0$. Put $c = \frac{\sigma^2 \xi}{2\sqrt{2\kappa\sigma\beta\gamma}}$. Then we get

$$\int \frac{e^{iA_0 \xi z}}{z} dz = I = i \int_{\frac{\pi}{4}}^{\frac{\pi}{4}+\pi} e^{c(1+i)r(\cos\theta + i\sin\theta)} d\theta$$

$$= i \int_{\frac{\pi}{4}}^{\frac{\pi}{4}+\pi} e^{cr[\cos\theta - \sin\theta + i(\cos\theta + \sin\theta)]} d\theta .$$

Hence

$$|I| < \int_{\frac{\pi}{4}}^{\frac{\pi}{4}+\pi} e^{cr(\cos\theta - \sin\theta)} d\theta$$

$$= \int_{\frac{\pi}{4}}^{\frac{\pi}{4}+\pi} e^{cr\sqrt{2}\sin\left(\frac{\pi}{4}-\theta\right)} d\theta = \int_0^{\pi} e^{-cr\sqrt{2}\sin\theta'} d\theta'$$

$$= 2\int_0^{\frac{\pi}{2}} e^{-cr\sqrt{2}\sin\theta'} d\theta' < 2\int_0^{\frac{\pi}{2}} e^{-\frac{2c\sqrt{2}r}{\pi}\theta} d\theta$$

$$= -\frac{\pi}{c\sqrt{2}r}\left[e^{-2\sqrt{2}cr} - 1\right].$$

Therefore, when $\xi > 0$, i.e. when $c > 0$, we get

$$\lim_{r\to\infty} I = 0 ,$$

and when $\xi = 0$, i.e. when $c = 0$, we get

$$\lim_{r\to\infty} I = 2\pi .$$

Hence, when $\xi > 0$, if we take a circular path as shown in Fig. 11 from $\theta = \frac{\pi}{4}$ to $\theta = \pi + \frac{\pi}{4}$, we get $\lim_{r\to\infty} I_{CP} = 0$.

(b) The case where $\xi \leqq 0$. In this case we carry out the integration along a large semi-circle on the other side of CP. Then

$$I' = \int \frac{e^{iA_0\xi z}}{z} dz = -i \int_{\frac{\pi}{4}+\pi}^{\frac{\pi}{4}+2\pi} e^{c(1+i)r(\cos\theta + i\sin\theta)} d\theta$$

$$= -i \int_{\frac{\pi}{4}}^{\frac{\pi}{4}+\pi} e^{-c(1+i)\, r(\cos\theta' + i\sin\theta')} d\theta' .$$

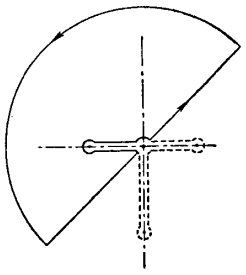

Fig. 12.

Hence

$$|I'| < \frac{\pi}{c\sqrt{2}\, r}\left[e^{2\sqrt{2}cr} - 1\right].$$

Therefore, when $\xi < 0$, i.e. when $c < 0$, we get

$$\lim_{r\to\infty} I' = 0 ,$$

and when $\xi = 0$, i.e. when $c = 0$, we get

$$\lim_{r\to\infty} I' = 2\pi .$$

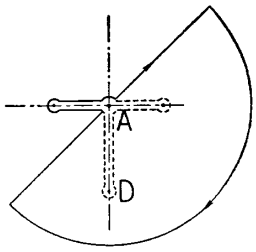

Fig. 13.

Hence, when $\xi < 0$, if we take a large circular path from $\theta = \frac{\pi}{4} + \pi$ to $\theta = \frac{\pi}{4} + 2\pi$, we get $\lim_{r\to\infty} I_{CP} = 0$.

In the above two cases, the value of the integral along the large semi-circle becomes indeterminate when $\xi = 0$, $\eta = h$. From the feregoing considerations, we see that the path of integration should be chosen as shown in Fig. 12, when $\xi \geqq 0$, and as shown in Fig. 13, when $\xi \leqq 0$, except when $\xi = 0$, $\eta = h$ in both cases.

D is the branch point of the function to be integrated, but is not the pole of that function. Hence the integration along a path twice round **D** is null, and the function returns to the original leaf of the Riemann surface after going twice round **D**; consequently, the integrations along **AD** and **DA** cancel each other.

We can carry out the integrations (5)—(7) in the same way on the third sheet as on the first sheet. The integrations (1)—(4) on the third sheet are carried out as follows:

(8) On $\mathbf{A'C}$, $z = re^{i\frac{\pi}{4}}$ and $\sqrt{1-z^2} = -\sqrt{1-ir^2}$, hence

$$I_{A'C} = -\int_0^\infty \frac{A_0 re^{i\frac{\pi}{4}} e^{iA_0 e^{i\frac{\pi}{4}} r\xi}}{\sinh re^{i\frac{\pi}{4}} A_1 \cdot \sqrt{1-ir^2}} \times \frac{\sinh A_0\sqrt{ir^2 - B(1-\sqrt{1-ir^2})}\,\eta}{\sinh A_0\sqrt{ir^2 - B(1-\sqrt{1-ir^2})}\,h} e^{i\frac{\pi}{4}} dr.$$

(9) On $\mathbf{AP}$, $z = re^{i\left(\frac{\pi}{4}+\pi\right)}$ and $\sqrt{1-z^2} = \sqrt{1-ir^2}$, hence

$$I_{PA} = \int_0^\infty \frac{A_0 re^{i\frac{\pi}{4}} e^{-iA_0 e^{i\frac{\pi}{4}} r\xi}}{\sinh re^{i\frac{\pi}{4}} A_1 \cdot \sqrt{1-ir^2}} \times \frac{\sinh A_0\sqrt{ir^2 - B(1+\sqrt{1-ir^2})}\,\eta}{\sinh A_0\sqrt{ir^2 - B(1+\sqrt{1-ir^2})}\,h} e^{i\frac{\pi}{4}} dr.$$

(10) On $\mathbf{AB}$, $z = -x$ and $\sqrt{1-z^2} = -\sqrt{1-x^2}$, hence

$$I_{AB} = \int_0^1 \frac{A_0 xe^{-iA_0 x\xi}}{\sinh xA_1 \cdot \sqrt{1-x^2}} \times \frac{\sinh A_0\sqrt{x^2 - B(1-\sqrt{1-x^2})}\,\eta}{\sinh A_0\sqrt{x^2 - B(1-\sqrt{1-x^2})}\,h} dx.$$

(11) On $\mathbf{A'B}$, $z = -x$ and $\sqrt{1-z^2} = \sqrt{1-x^2}$, hence

$$I_{BA'} = \int_0^1 \frac{A_0 xe^{-iA_0 x\xi}}{\sinh xA_1 \cdot \sqrt{1-x^2}} \times \frac{\sinh A_0\sqrt{x^2 - B(1+\sqrt{1-x^2})}\,\eta}{\sinh A_0\sqrt{x^2 - B(1+\sqrt{1-x^2})}\,h} dx.$$

(12) If we add the integrals on the first sheet and those on the third sheet together, we obtain

$$2\int_0^\infty \frac{A_0 re^{i\frac{\pi}{4}} \cos(A_0 e^{i\frac{\pi}{4}} r\xi)}{\sinh re^{i\frac{\pi}{4}} A_1 \cdot \sqrt{1-ir^2}} \left\{ \frac{\sinh A_0\sqrt{ir^2 - B(1+\sqrt{1-ir^2})}\,\eta}{\sinh A_0\sqrt{ir^2 - B(1+\sqrt{1-ir^2})}\,h} - \frac{\sinh A_0\sqrt{ir^2 - B(1-\sqrt{1-ir^2})}\,\eta}{\sinh A_0\sqrt{ir^2 - B(1-\sqrt{1-ir^2})}\,h} \right\} e^{i\frac{\pi}{4}} dr. \qquad (12)$$

The paths of the integration should be chosen as shown in Fig. 12, when $\xi \geqq 0$, and as shown in Fig. 13, when $\xi \leqq 0$. The value of this integral is equal to $2\pi i$ times the sum of the residues within the contour. We next calculate the residues.

As explained above, $\zeta = \pm nMe^{-i\frac{\pi}{4}}$ are the poles of $\frac{1}{\sinh A_0 h\zeta}$, with an ecception of $n = 0$, at which it is the branch point, but not a pole.

(13) Let the points in the z-plane corresponding to $\zeta = \pm nMe^{-i\frac{\pi}{4}}$ be expressed by $z_{\pm n}$. Their positions in the z-plane are shown in Fig. 10, from which we see that, when $\xi \gtrless 0$, we have to consider z_n on the first sheet, and z_{-n} on the third sheet.

Let

$$f(z) = \frac{A_0 z e^{iA_0 z\xi}}{\sinh A_1 z \cdot \sqrt{1-z^2}} \times \frac{\sinh A_0 \sqrt{z^2 - B(1+\sqrt{1-z^2})}\,\eta}{\sinh A_0 \sqrt{z^2 - B(1+\sqrt{1-z^2})}\,h},$$

and again put

$$f(z) = \frac{P(z)}{\sinh A_0 \sqrt{z^2 - B(1+\sqrt{1-z^2})}\,h}.$$

Then, since

$$\lim_{\zeta \to \pm nMe^{-i\frac{\pi}{4}}} \frac{\zeta \mp nMe^{-i\frac{\pi}{4}}}{\sinh A_0 \zeta h} = \lim_{\zeta' \to 0} \frac{\zeta'}{\sinh A_0 h\,(\zeta' \pm nMe^{-i\frac{\pi}{4}})}$$

$$= \lim_{\zeta' \to 0} \frac{1}{A_0 h \cosh A_0 h(\zeta' \pm nMe^{-i\frac{\pi}{4}})} = \frac{1}{A_0 h \cosh A_0 h n Me^{-i\frac{\pi}{4}}}$$

$$= \frac{1}{A_0 h \cos n\pi} = (-1)^n \frac{1}{A_0 h},$$

we get

$$\operatorname*{Res}_{z=z_{\pm n}} f(z) = \frac{P(z_{\pm n})}{Ah}(-1)^n,$$

and since

$$\sinh(A_0 \eta \zeta_{\pm n}) = \sinh\left[\pm A_0 \eta M \frac{hne^{-i\frac{\pi}{4}}}{h}\right] = \sinh\left[\mp in\pi\frac{\eta}{h}\right]$$

$$= \pm i \sin\left(n\pi\frac{\eta}{h}\right),$$

we get

$$\operatorname*{Res}_{z=z_{\pm n}} f(z) = \pm i \frac{e^{iA_0 z_{\pm n}\xi}}{\sqrt{1-z_{\pm n}^2}} \sin\left(n\pi\frac{\eta}{h}\right)\frac{z_{\pm n}}{h \sinh A_1 z_{\pm n}}(-1)^n .$$

Therefore, when $\xi \geqq 0$, the sum of the residues within the contours on the first sheet and on the third sheet is

$$i\sum_{n=1}^{\infty}(-1)^n \sin\left(n\pi\frac{\eta}{h}\right)\left[\frac{e^{iA_0 z_n \xi} z_n}{\sinh A_1 z_n \sqrt{1-z_n^2}} - \frac{e^{iA_0 z_{-n}\xi} z_{-n}}{\sinh A_1 z_{-n}\sqrt{1-z_n^2}}\right]\frac{1}{h},$$

where

$$z_{\pm n} = \sqrt{\frac{2\beta\gamma}{\sigma_2}\left[\left(1-\frac{\beta\gamma}{\sigma^2}\right) \pm \sqrt{\left(\frac{\beta\gamma}{\sigma^2}-1\right) + in^2M^2}\right] - in^2M^2} .$$

(14) We next calculate the residues at the points where the equation $\sinh A_1 z = 0$ is satisfied.

The equation

$$\sinh A_1 z = \sinh \frac{\pi}{b} A_0 z = -i \sin\left(iA_0\frac{\pi}{b}z\right) = 0$$

is satisfied at the points

$$iA_0\frac{\pi}{b}z = \pm n\pi .$$

Let these points be denoted by $\bar{z}_{\pm n}$. Then we obtain

$$\bar{z}_{\pm n} = \pm\frac{n\pi}{iA_0\frac{\pi}{b}} = \pm\frac{nb}{iA_0} = \pm\frac{2nb\sqrt{\kappa\sigma\beta\gamma}}{\sigma^2}e^{-i\frac{\pi}{4}} = \pm nDe^{-i\frac{\pi}{4}} \text{ (say).}$$

Hence $\bar{z}_n$ lie in the fourth quadrant and $\bar{z}_{-n}$ in the second quadrant. Therefore, when $\xi \geqq 0$, the contour encloses $\bar{z}_{-n}$ only, so we calculate the residues of $f(z)$ within this contour.

Since

$$\lim_{z\to\bar{z}_{-n}} \frac{z-\bar{z}_{-n}}{\sinh A_0\frac{\pi z}{b}} = \lim_{z\to\bar{z}_{-n}} \frac{1}{A_0\frac{\pi}{b}\cosh A_0\frac{\pi z}{b}} = \frac{1}{A_0\frac{\pi}{b}\cosh A_0\frac{\pi}{b}\frac{nb}{iA_0}}$$

$$= \frac{1}{A_0\frac{\pi}{b}\cosh\frac{n\pi}{i}} = \frac{1}{A_0\frac{\pi}{b}\cos n\pi} = (-1)^n\frac{b}{\pi A_0},$$

we get

$$\operatorname*{Res}_{z=\bar{z}_{-n}} f(z) = (-1)^{n+1}\frac{bnDe^{-i\frac{\pi}{4}}e^{-iA_0^2nDe^{-i\frac{\pi}{4}}}}{\pm\pi\sqrt{1+in^2D^2}}$$

$$\times\frac{\sinh A_0\sqrt{-in^2D^2-B(1\pm\sqrt{1+in^2D^2})}\eta}{\sinh A_0\sqrt{-in^2D^2-B(1\pm\sqrt{1+in^2D^2})}h},$$

where

$$A_0 = \frac{\sigma^2}{2\sqrt{\kappa\sigma\beta\gamma}}e^{-i\frac{\pi}{4}}, \quad D = \frac{2b\sqrt{\kappa\sigma\beta\gamma}}{\sigma^2}, \quad B = \frac{2\beta\gamma}{\sigma_2}$$

and, of the double sign, positive sign should be taken on the first sheet and the negative sign on the third sheet. Therefore

$$A_0D = -ibe^{i\frac{\pi}{4}} \text{ consequently } A_0D^2 = -ib^2,$$

hence

$$-in^2D^2A_0^2-A_0^2B(1\pm\sqrt{1+in^2D^2})$$

$$= -n^2b^2+\frac{i\sigma^2}{2\kappa\sigma}\left(1\pm\sqrt{1+in^2\frac{4b^2\kappa\sigma\beta\gamma}{\sigma^4}}\right)$$

$$= -n^2b^2-\frac{\sigma^2\pm\sqrt{\sigma^4+4i\kappa\sigma\beta\gamma n^2b^2}}{2i\kappa\sigma}.$$

Therefore, if we put

$$e_1^2 = -n^2b^2 - \frac{\sigma^2 + \sqrt{\sigma^4 + 4i\kappa\sigma\beta\gamma n^2b^2}}{2i\kappa\sigma},$$

$$e_2^2 = -n^2b^2 - \frac{\sigma^2 - \sqrt{\sigma^4 + 4i\kappa\sigma\beta\gamma n^2b^2}}{2i\kappa\sigma},$$

we may write

$$\operatorname*{Res}_{z=\tilde{z}_{-n}} f(z) = \sum_{n=1}^{\infty} \frac{2b\sqrt{\kappa\sigma\beta\gamma}}{\pi e^{i\frac{\pi}{4}}}(-1)^{n+1} \frac{nbe^{-nb\xi}}{\sqrt{\sigma^4 + 4i\kappa\sigma\beta\gamma n^2b^2}} \times \left\{ \frac{\sinh e_1\eta}{\sinh e_1 h} - \frac{\sinh e_2\eta}{\sinh e_2 h} \right\}.$$

The signs of e_1 and e_2 are determined from Fig. 8.

(15) From (12) we get

$$A_0 e^{i\frac{\pi}{4}} r = a, \quad ir^2 = \frac{a^2}{A_0^2}, \quad \text{and} \quad 1 - \frac{a^2}{A_0^2} = \frac{1}{\sigma^4}[\sigma^4 - 4i\kappa\sigma\beta\gamma a^2].$$

Hence we have

$$2\int_0^{\infty} \frac{A_0 r e^{i\frac{\pi}{4}} \cos(A_0\xi e^{i\frac{\pi}{4}} r)}{\sinh r A_0 \frac{\pi}{b} e^{i\frac{\pi}{4}} \cdot \sqrt{1 - ir^2}} \left\{ \frac{\sinh A_0\sqrt{ir^2 - B(1+\sqrt{1-ir^2})}\eta}{\sinh A_0\sqrt{ir^2 - B(1+\sqrt{1-ir^2})}h} - \frac{\sinh A_0\sqrt{ir^2 - B(1-\sqrt{1-ir^2})}\eta}{\sinh A_0\sqrt{ir^2 - B(1-\sqrt{1-ir^2})}h} \right\} e^{i\frac{\pi}{4}} dr$$

$$= 2\int_0^{\infty} \frac{a e^{i\frac{\pi}{4}} 2\sqrt{\kappa\sigma\beta\gamma}\cos a\xi}{\sinh\frac{\pi a}{b}\sqrt{\sigma^4 - 4i\kappa\sigma\beta\gamma a^2}} \left\{ \frac{\sinh c_1\eta}{\sinh c_1 h} - \frac{\sinh c_2\eta}{\sinh c_2 h} \right\} da.$$

Therefore, when $\xi \gtrless 0$, we obtain

$$\int_0^\infty \frac{a\cos a\xi}{\sinh\frac{\pi a}{b}\sqrt{\sigma^4-4i\kappa\sigma\beta\gamma a^2}}\left\{\frac{\sinh c_1\eta}{\sinh c_1 h}-\frac{\sinh c_2\eta}{\sinh c_2 h}\right\}da$$

$$=\frac{\pi}{2\sqrt{\kappa\sigma\beta\gamma}}e^{-i\frac{\pi}{4}}\sum_{n=1}^{\infty}(-1)^{n+1}\sin\left(n\pi\frac{\eta}{h}\right)\left[\frac{z_n e^{iA_0 z_n\xi}}{\sinh A_1 z_n\cdot\sqrt{1-z_n^2}}\right.$$

$$\left.-\frac{z_{-n}e^{iA_0 z_{-n}\xi}}{\sinh A_1 z_{-n}\cdot\sqrt{1-z_{-n}^2}}\right]\frac{1}{h}$$

$$+\sum_{n=1}^{\infty}(-1)^{n+1}\frac{nb^2e^{-nb\xi}}{\sqrt{\sigma^4+4i\kappa\sigma\beta\gamma n^2b^2}}\left\{\frac{\sinh e_1\eta}{\sinh e_1 h}-\frac{\sinh e_2\eta}{\sinh e_2 h}\right\}.$$

(16) When $\xi<0$, we have to take z_{-n} on the first sheet and z_{+n} on the third sheet. Hence the sum of the residues in the region considered is

$$i\sum_{n=1}^{\infty}(-1)^n\sin\left(n\pi\frac{\eta}{h}\right)\left\{\frac{e^{iA_0 z'_n\xi}z'_n}{\sinh A_1 z'_n\cdot\sqrt{1-z'^2_n}}-\frac{e^{iA_0 z'_{-n}\xi}z'_{-n}}{\sinh A_1 z'_{-n}\cdot\sqrt{1-z'^2_{-n}}}\right\},$$

where $z'_{\pm n}=-z_{\pm n}$.

Similarly, in calculating the residues of $f(z)$ at the points corresponding to the roots of the equation $\sinh A_1 z=0$, we have to choose such roots, at which $z=\bar{z}_n$.

$$\sum_{z=\bar{z}_n}\mathrm{Res}=-\sum_{n=1}^{\infty}\frac{2b\sqrt{\kappa\sigma\beta\gamma}}{\pi e^{i\frac{\pi}{4}}}(-1)^{n+1}\frac{nbe^{nb\xi}}{\sqrt{\sigma^4+4i\kappa\sigma\beta\gamma n^2b^2}}$$

$$\times\left\{\frac{\sinh e_1\eta}{\sinh e_1 h}-\frac{\sinh e_2\eta}{\sinh e_2 h}\right\}.$$

When $\xi<0$, since the path of integration is taken in the negative sense, the contour integral is equal to $-2\pi i$ times the sum of the residues.

(17) Therefore, when $\xi<0$, we obtain

$$\int_0^\infty \frac{a\cos a\xi}{\sinh\frac{\pi a}{b}\sqrt{\sigma^4-4i\kappa\sigma\beta\gamma a^2}}\left\{\frac{\sinh c_1\eta}{\sinh c_1 h}-\frac{\sinh c_2\eta}{\sinh c_2 h}\right\}da$$

$$=\frac{\pi}{2\sqrt{\kappa\sigma\beta\gamma}}e^{-i\frac{\pi}{4}}\sum_{n=1}^{\infty}(-1)^{n+1}\sin\left(n\pi\frac{\eta}{h}\right)\left[\frac{z_n e^{-iA_0 z_n\xi}}{\sinh A_1 z_n\cdot\sqrt{1-z_n^2}}\right.$$

$$\left.-\frac{z_{-n}e^{-iA_0 z_{-n}\xi}}{\sinh A_1 z_{-n}\cdot\sqrt{1-z_{-n}^2}}\right]\frac{1}{h}$$

$$+\sum_{n=1}^{\infty}(-1)^{n+1}\frac{nbe^{-nb\xi}}{\sqrt{\sigma^4+4i\kappa\sigma\beta\gamma n^2b^2}}\left\{\frac{\sinh e_1\eta}{\sinh e_1 h}-\frac{\sinh e_2\eta}{\sinh e_2 h}\right\}.$$

[II] We next perform the integration

$$\int_0^\infty \frac{\cos a\xi}{\sqrt{\sigma^4-4i\kappa\sigma\beta\gamma a^2}}\left[\frac{\sinh c_1\eta}{\sinh c_1 h}-\frac{\sinh c_2\eta}{\sinh c_2 h}\right]da,$$

which appears in the expression for ψ

In this case, since $\xi=R-x$ is always positive, we perform the integration

$$I=\int\frac{e^{iA_0 z\xi}}{\sqrt{1-z^2}}\frac{\sinh A_0\sqrt{z^2-B(1+\sqrt{1-z^2})}\eta}{\sinh A_0\sqrt{z^2-B(1+\sqrt{1-z^2})}h}dz$$

in the same region as that in the case where $\xi\geqq 0$, as described above. In the same way as in the former case, we get the sum of the integrals on the first sheet and on the third sheet thus:

$$2\int_0^\infty \frac{\cos A_0 e^{i\frac{\pi}{4}}r\xi}{\sqrt{1-ir^2}}\left\{\frac{\sinh A_0\sqrt{ir^2-B(1+\sqrt{1-ir^2})}\eta}{\sinh A_0\sqrt{ir^2-B(1+\sqrt{1-ir^2})}h}\right.$$

$$\left.-\frac{\sinh A_0\sqrt{ir^2-B(1-\sqrt{1-ir^2})}\eta}{\sinh A_0\sqrt{ir^2-B(1-\sqrt{1-ir^2})}h}\right\}e^{i\frac{\pi}{4}}dr$$

$$=2\frac{\sigma^2}{A_0}\int_0^\infty\frac{\cos a\xi}{\sqrt{\sigma^4-4i\kappa\sigma\beta\gamma a^2}}\left\{\frac{\sinh c_1\eta}{\sinh c_1 h}-\frac{\sinh c_2\eta}{\sinh c_2 h}\right\}da$$

$$=2\pi\sum_{n=1}^{\infty}(-1)^{n+1}\sin\left(n\pi\frac{\eta}{h}\right)\left[\frac{e^{iA_0 z_n\xi}}{\sqrt{1-z_n^2}}-\frac{e^{iA_0 z_{-n}\xi}}{\sqrt{1-z_{-n}^2}}\right]\frac{1}{A_0 h}.$$

Hence

$$\int_0^\infty \frac{\cos a\xi}{\sqrt{\sigma^4-4i\kappa\sigma\beta\gamma a^2}}\left\{\frac{\sinh c_1\eta}{\sinh c_1 h}-\frac{\sinh c_2\eta}{\sinh c_2 h}\right\}da$$

$$=\frac{\pi}{h\sigma^2}\sum_{n=1}^{\infty}(-1)^{n+1}\sin\left(n\pi\frac{\eta}{h}\right)\left[\frac{e^{iA_0z_n\xi}}{\sqrt{1-z_n^2}}-\frac{e^{iA_0z_{-n}\xi}}{\sqrt{1-z_{-n}^2}}\right], \quad (13)$$

where $\xi=R-x$ and R is to be made infinitely great. When $\xi\geqq 0$, as shown in Fig. 12, the real parts of both z_{+n} (on the first sheet) and z_{-n} (on the third sheet) are negative, and the imaginary part of z_n (on the first sheet) is negative when n is small and positive when n is large. In any case, if we put $z_{\pm n}=\mu+i\nu$, $\mu-\nu$ is negative. Hence

$$\Re iA_0z_{\pm n}\xi=\Re i\frac{\sigma^2}{2\sqrt{\kappa\sigma\beta\gamma}}e^{-i\frac{\pi}{4}}(\mu+i\nu)\xi=\frac{\sigma^2}{2\sqrt{\kappa\sigma\beta\gamma}}\xi(\mu-\nu)<0.$$

Therefore we get

$$\lim_{\xi\to\infty}e^{iA_0z_{\pm n}\xi}=0,$$

and ξ is infinity as long as x is finite. Hence the integral (13) vanishes.

[III] From the foregoing calculations, we obtain the expression for ψ as follows:

$$\psi=\Im\left\{C\gamma e^{i\sigma t}\sum_{n=1}^{\infty}(-1)^{n+1}e^{\pm nbx}\frac{i\kappa nb}{\sqrt{\sigma^4+4i\kappa\sigma\beta\gamma n^2b^2}}\right.$$

$$\times\left[\frac{\sinh e_1(h-y)}{\sinh e_1h}-\frac{\sinh e_2(h-y)}{\sinh e_2h}\right]$$

$$+C\frac{\pi}{2h}\sqrt{\frac{\kappa\gamma}{\sigma\beta}}e^{i\frac{\pi}{4}}\sum_{n=1}^{\infty}(-1)^{n+1}\sin\left(n\pi\frac{h-y}{h}\right)$$

$$\left.\times\left[\frac{z_ne^{\mp iA_0z_nx}}{\sinh A_1z_n\cdot\sqrt{1-z_n^2}}-\frac{z_{-n}e^{\mp iA_0z_{-n}x}}{\sinh A_1z_{-n}\cdot\sqrt{1-z_{-n}^2}}\right]\right\}, \quad (14)$$

and, of the double signs, upper signs should be taken for $x<0$, and lower signs for $x>0$, and

$$A_0 = \frac{\sigma^2}{2\sqrt{\kappa\sigma\beta\gamma}} e^{-i\frac{\pi}{4}}, \qquad A_1^* = \frac{\pi}{b} A_0,$$

$$z_{\pm n} = \sqrt{\frac{2\beta\gamma}{\sigma^2}\left[\left(1-\frac{\beta\gamma}{\sigma^2}\right) \pm \sqrt{\left(\frac{\beta\gamma}{\sigma^2}-1\right)^2 + in^2M^2}\right] - in^2M^2},$$

where

$$M = \frac{\pi}{h}\frac{2\sqrt{\kappa\sigma\beta\gamma}}{\sigma^2},$$

$$\left.\begin{aligned} e_1^2 &= -n^2b^2 - \frac{\sigma^2 + \sqrt{\sigma^4 + 4i\kappa\sigma\beta\gamma n^2b^2}}{2\kappa i\sigma}, \\ e_2^2 &= -n^2b^2 - \frac{\sigma^2 - \sqrt{\sigma^4 + 4i\kappa\sigma\beta\gamma n^2b^2}}{2\kappa i\sigma}. \end{aligned}\right\} \qquad (14')$$

[IV] We next perform the integrations in the expression for ϑ.

(1) In the first place, consider the integral

$$I = \int_0^\infty \frac{\sin ax}{\sinh\frac{\pi a}{b}\sqrt{\sigma^4 - 4i\kappa\sigma\beta\gamma a^2}} \times \left\{(c_1^2-a^2)\frac{\sinh c_1(y-h)}{\sinh c_1 h} - (c_2^2-a^2)\frac{\sinh c_2(y-h)}{\sinh c_2 h}\right\} da$$

$$= -\frac{\sigma}{2\kappa i}\int_0^\infty \frac{\sin ax}{\sinh\frac{\pi a}{b}\sqrt{\sigma^4 - 4i\kappa\sigma\beta\gamma a^2}} \times \left\{\frac{\sinh c_1(y-h)}{\sinh c_1 h} - \frac{\sinh c_2(y-h)}{\sinh c_2 h}\right\} da$$

$$-\frac{1}{2\kappa i\sigma}\int_0^\infty \frac{\sin ax}{\sinh\frac{\pi a}{b}}\left\{\frac{\sinh c_1(y-h)}{\sinh c_1 h} + \frac{\sinh c_2(y-h)}{\sinh c_2 h}\right\} da.$$

Let the first integral on the right hand side be H. Then

$$\frac{\partial H}{\partial x} = \int_0^\infty \frac{a \cos ax}{\sinh \frac{\pi a}{b} \sqrt{\sigma^4 - 4i\kappa\sigma\beta\gamma a^2}} \times \left\{ \frac{\sinh c_1(y-h)}{\sinh c_1 h} - \frac{\sinh c_2(y-h)}{\sinh c_2 h} \right\} da ,$$

which is equal to the integral (11). Hence

$$H = \int dx \int_0^\infty \frac{a \cos ax}{\sinh \frac{\pi a}{b} \sqrt{\sigma^4 - 4i\kappa\sigma\beta\gamma a^2}} \times \left\{ \frac{\sinh c_1(y-h)}{\sinh c_1 h} - \frac{\sinh c_2(y-h)}{\sinh c_2 h} \right\} da + F(y) .$$

We can evaluate H from the contour integral

$$I' = \int \frac{e^{iA_0\xi z}}{\sinh A_1 z \cdot \sqrt{1-z^2}} \times \frac{\sinh A_0 \sqrt{z^2 - B(1+\sqrt{1-z^2})}\,\eta}{\sinh A_0 \sqrt{z^2 - B(1+\sqrt{1-z^2})}\,h} dz$$

in the same region as in [I], and $F(y)$ can be calculated from the contour integral round a small circle about $z = 0$. In the case of [I], this contour integral about $z = 0$ vanishes, but, in the latter case, it does not vanish as proved in the following.

(2) Next perform the integration

$$\int_0^\infty \frac{\sin ax}{\sinh \frac{\pi a}{b}} \left\{ \frac{\sinh c_1(y-h)}{\sinh c_1 h} - \frac{\sinh c_2(y-h)}{\sinh c_2 h} \right\} da .$$

For the sake of carrying out the above integration, we perform the contour integral

$$I = \int \frac{e^{iA_0 z\xi}}{\sinh A_1 z} \frac{\sinh A_0 \sqrt{z^2 - B(1+\sqrt{1-z^2})}\,\eta}{\sinh A_0 \sqrt{z^2 - B(1+\sqrt{1-z^2})}\,h} dz$$

in the same region as in the case of [I]. On the first sheet we get

$$I_{A'C} = \int_0^\infty \frac{e^{iA_0 e^{i\frac{\pi}{4}} r\xi}}{\sinh r e^{i\frac{\pi}{4}} A_1} \frac{\sinh A_0 \sqrt{ir^2 - B(1+\sqrt{1-ir^2})}\,\eta}{\sinh A_0 \sqrt{ir^2 - B(1+\sqrt{1-ir^2})}\,h} e^{i\frac{\pi}{4}} dr$$

and

$$I_{PA} = -\int_0^\infty \frac{e^{-iA_0 e^{i\frac{\pi}{4}} r\xi}}{\sinh r e^{i\frac{\pi}{4}} A_1} \frac{\sinh A_0\sqrt{ir^2 - B(1-\sqrt{1-ir^2})\eta}}{\sinh A_0\sqrt{ir^2 - B(1-\sqrt{1-ir^2})h}} e^{i\frac{\pi}{4}} dr$$

and, on the third sheet we get

$$I_{A'C} = \int_0^\infty \frac{e^{iA_0 e^{i\frac{\pi}{4}} r\xi}}{\sinh r e^{i\frac{\pi}{4}} A_1} \frac{\sinh A_0\sqrt{ir^2 - B(1-\sqrt{1-ir^2})\eta}}{\sinh A_0\sqrt{ir^2 - B(1-\sqrt{1-ir^2})h}} e^{i\frac{\pi}{4}} dr$$

and

$$I_{PA} = -\int_0^\infty \frac{e^{-iA_0 e^{i\frac{\pi}{4}} r\xi}}{\sinh r e^{i\frac{\pi}{4}} A_1} \frac{\sinh A_0\sqrt{ir^2 - B(1+\sqrt{1-ir^2})\eta}}{\sinh A_0\sqrt{ir^2 - B(1+\sqrt{1-ir^2})h}} e^{i\frac{\pi}{4}} dr .$$

We have also

$$\overbrace{I_{AB} + I_{BA'}}^{\text{First sheet}} + \overbrace{I_{AB} + I_{BA'}}^{\text{Third sheet}} = 0 .$$

As in the case of [I], the region of the complex integration when $\xi > 0$ differs from that when $\xi < 0$. It can be easily proved that the complex integral along a small circle about **B** vanishes as in [I]. Hence we obtain

$$\overbrace{I_{A'C} + I_{PA}}^{\text{First sheet}} + \overbrace{I_{A'C} + I_{PA}}^{\text{Third sheet}}$$

$$= 2i\int_0^\infty \frac{\sin A_0 e^{i\frac{\pi}{4}} r\xi}{\sinh A_1 r e^{i\frac{\pi}{4}}} \left\{ \frac{\sinh A_0\sqrt{ir^2 - B(1+\sqrt{1-ir^2})\eta}}{\sinh A_0\sqrt{ir^2 - B(1+\sqrt{1-ir^2})h}} + \frac{\sinh A_0\sqrt{ir^2 - B(1-\sqrt{1-ir^2})\eta}}{\sinh A_0\sqrt{ir^2 - B(1-\sqrt{1-ir^2})h}} \right\} e^{i\frac{\pi}{4}} dr$$

$$= \frac{2i}{A}\int_0^\infty \frac{\sin a\xi}{\sinh\frac{\pi a}{b}} \left\{ \frac{\sinh c_1\eta}{\sinh c_1 h} + \frac{\sinh c_2\eta}{\sinh c_2 h} \right\} da$$

$$= \pm 2\pi i \sum \text{Res } f(z) + I_{\text{at } z=0} ,$$

where positive sign should be taken when $\xi \gtrless 0$, and negative sign when $\xi \lesssim 0$. We can calculate the residues in the same way as in the cases (13) and (14) in [I]. $I_{\text{at } z=0}$ will be calculated afterwards.

From these calculations we obtain

$$I = \int_0^\infty \frac{\sin ax}{\sinh \frac{\pi a}{b}\sqrt{\sigma^4 - 4i\kappa\sigma\beta\gamma a^2}} \times \left\{(c_1^2 - a^2)\frac{\sinh c_1(y-h)}{\sinh c_1 h} - (c_2^2 - a^2)\frac{\sinh c_2(y-h)}{\sinh c_2 h}\right\} da$$

$$= \pm \sum_{n=1}^{\infty} (-1)^n e^{\pm nbx} \frac{b}{\sqrt{\sigma^4 + 4\,i\kappa\sigma\beta\gamma n^2 b^2}} \times \left\{(n^2b^2 + e_1^2)\frac{\sinh e_1(y-h)}{\sinh e_1 h} - (n^2b^2 + e_2^2)\frac{\sinh e_2(y-h)}{\sinh e_2 h}\right\}$$

$\pm$ (Integral round a small semi-circle about $z = 0$)

$$\mp \frac{\pi b\gamma}{h\sigma^3} \sum_{n=1}^{\infty} (-1)^{n+1} \sin\left(n\pi \frac{y-h}{h}\right) \left\{\left(\frac{n^2\pi^2}{h^2} + A_0^2 z_n^2\right)\frac{e^{\mp iA_0 z_n x}}{\sinh A_1 z_n \sqrt{1 - z_n^2}} - \left(\frac{n^2\pi^2}{h^2} + A_0^2 z_{-n}^2\right)\frac{e^{\mp iA_0 z_{-n} x}}{\sinh A_1 z_{-n}\sqrt{1 - z_{-n}^2}}\right\},$$

where the upper sign should be taken for $\xi \lesssim 0$ and the lower sign for $\xi \gtrless 0$. When $\xi < 0$, we have to integrate twice round **D**, but the integral vanishes. This integral corresponds to the case $n = 0$ in the last term of the above expression.

(3) We have now to carry out the complex integration along a small semi-circle around $z = 0$. It is convenient to perform the integrations in the cases (1) and (2) simultaneously.

Now integrate

$$I = \int \frac{e^{iA_0\xi z}}{\sinh A_1 z\sqrt{1 - z^2}} \left[-\frac{\sigma(1 + \sqrt{1 - z^2})}{2i\kappa}\right] \frac{\sinh A_0\sqrt{z^2 - B(1 + \sqrt{1 - z^2})}\,\eta}{\sinh A_0\sqrt{z^2 - B(1 + \sqrt{1 - z^2})}\,h} dz$$

along a small semi-circle around $z=0$ on the first and third sheets.

On the first sheet we have

$$\lim_{z\to 0}\frac{e^{iA_0\xi z}}{\sqrt{1-z^2}}\left[-\frac{\sigma(1+\sqrt{1-z^2})}{2i\kappa}\right]\frac{\sinh A_0\sqrt{z^2-B(1+\sqrt{1-z^2})}\,\eta}{\sinh A_0\sqrt{z^2-B(1+\sqrt{1-z^2})}\,h}$$

$$=-\frac{\sigma}{i\kappa}\frac{\sinh iA_0\sqrt{2B}\eta}{\sinh iA_0\sqrt{2B}h}$$

and

$$\lim_{z\to 0}\frac{z}{\sinh A_1 z}=\frac{1}{A_1}.$$

Hence we get

$$I=\mp\pi i\frac{\sigma}{i\kappa}\frac{1}{A_1}\frac{\sin A_0\sqrt{2B}\eta}{\sin A_0\sqrt{2B}h}=\mp\frac{\pi\sigma}{\kappa A_1}\frac{\sin A_0\sqrt{2B}\eta}{\sin A_0\sqrt{2B}h},$$

where negative sign is taken for $\xi\geqq 0$ and positive sign for $\xi\leqq 0$.

On the third sheet we have

$$\lim_{z\to 0}(1+\sqrt{1-z^2})=0.$$

Hence we get

$$I=0.$$

(4) We next carry out the integration

$$I=\int_0^\infty\frac{\sin a(R-x)}{a\sqrt{\sigma^4-4i\kappa\sigma\beta\gamma a^2}}$$

$$\times\left[(c_1^2-a^2)\frac{\sinh c_1(y-h)}{\sinh c_1 h}-(c_2^2-a^2)\frac{\sinh c_2(y-h)}{\sinh c_2 h}\right]da$$

In this case the calculation can be made in the same way as that in the case [II]. The value of the integral tends to the same value as that obtained by integrating along the semi-circle round A, when R tends to infinity.

Integrate

$$I'=\int\frac{e^{iA_0\xi z}}{z\sqrt{1-z^2}}\left[-\frac{\sigma(1+\sqrt{1-z^2})}{2i\kappa}\right]\frac{\sinh A_0\sqrt{z^2-B(1+\sqrt{1-z^2})}\,\eta}{\sinh A_0\sqrt{z^2-B(1+\sqrt{1-z^2})}\,h}dz$$

along a small semi-circle around A, then, since ξ is always positive in this case, we get

$$I'=-\frac{\pi\sigma}{\kappa}\frac{\sin A_0\sqrt{2B}\,\eta}{\sin A_0\sqrt{2B}\,h}.$$

Hence we obtain

$$I=-\frac{\pi}{2i\kappa\sigma}\frac{\sin A_0\sqrt{2B}\,\eta}{\sin A_0\sqrt{2B}\,h}.$$

From the foregoing calculations we obtain the expression for ϑ as follows:

$$\begin{aligned}\vartheta=\pm\Re\Bigg\{&Ce^{i\sigma t}\sum_{n=1}^{\infty}(-1)^n e^{\pm nbx}\frac{\kappa\sigma}{\sqrt{\sigma^4+4i\kappa\sigma\beta\gamma n^2b^2}}\\&\times\left[(n^2b^2+e_1^2)\frac{\sinh e_1(h-y)}{\sinh e_1h}-(n^2b^2+e_2^2)\frac{\sinh e_2(h-y)}{\sinh e^2h}\right]\\&-\frac{C}{2i}e^{i\sigma t}\frac{\sin A_0\sqrt{2B}(h-y)}{\sin A_0\sqrt{2B}\,h}\Bigg\}+\Re\frac{C}{2i}e^{i\sigma t}\frac{\sin A_0\sqrt{2B}(h-y)}{\sin A_0\sqrt{2B}\,h}\\&\pm\Re\frac{C\kappa\gamma}{h\sigma^2}e^{i\sigma t}\sum_{n=1}^{\infty}(-1)^{n+1}\sin\left(n\pi\frac{h-y}{h}\right)\\&\times\left[\left(\frac{n^2\pi^2}{h^2}+A_0^2z_n^2\right)\frac{e^{\mp iA_0z_nx}}{\sinh A_1z_n\sqrt{1-z_n^2}}\right.\\&\left.-\left(\frac{n^2\pi^2}{h^2}-A_0^2z_{-n}^2\right)\frac{e^{\mp iA_0z_{-n}x}}{\sinh A_1z_{-n}\sqrt{1-z_{-n}^2}}\right]\end{aligned}\qquad(15)$$

where the upper sign should be taken when $x\leqq 0$, and the lower sign when $x\geqq 0$.

[V] We will assume the numerical values of the constants as follows, which are reasonable values in the case of land and sea breezes:

$$\kappa = 4{\cdot}5 \times 10^{7}, \qquad \beta = 3{\cdot}5 \times 10^{-5}, \qquad \sigma = 7{\cdot}3 \times 10^{-5},$$

$$\gamma = 3{\cdot}6, \qquad b = 10^{-6}, \qquad h = 9 \times 10^{5}.$$

Then, in the expression (14),

$$\sqrt{\frac{\kappa\gamma}{\sigma\beta}} = 2{\cdot}52 \times 10^{6} \quad \text{and} \quad \frac{1}{h}\sqrt{\frac{\kappa\gamma}{\sigma\beta}} = 2{\cdot}27.$$

When n is small,

$$z_{\pm n} \approx \frac{\beta\gamma}{\sigma^2}\sqrt{-2} = i\, 3{\cdot}35 \times 10^{7},$$

Hence

$$\left| e^{iA_0 z_n x} \right| \approx e^{-\frac{1}{2}\sqrt{\frac{\beta\gamma}{\sigma\kappa}}x} = e^{-1{\cdot}96 \times 10^{-3}x},$$

$$\frac{z_{\pm n}}{\sqrt{1 - z_{\pm n}^2}} \approx i,$$

and $$A_1 z_{\pm n} = 4{\cdot}36 \times 10^{6} \times e^{i\frac{\pi}{4}} = (1+i) \times 3{\cdot}08 \times 10^{6}.$$

Hence

$$\left| e^{-A_1 z_n} \right| = e^{-3{\cdot}08 \times 10^{6}}.$$

Therefore,

$$\left| \frac{\pi}{2h}\sqrt{\frac{\kappa\gamma}{\sigma\beta}} \left[\frac{z_n e^{\mp iA_0 z_n x}}{\sinh A_1 z_n \cdot \sqrt{1 - z_n^2}} - \frac{z_{-n} e^{\mp iA_0 z_{-n} x}}{\sinh A_1 z_{-n} \cdot \sqrt{1 - z_{-n}^2}} \right] \right|$$

is a quantity of the order $3{\cdot}57 \times e^{-3{\cdot}08 \times 10^{6}} \times e^{-1{\cdot}96 \times 10^{-3}x}$, while

$$\left| \frac{\gamma\kappa i n b \cdot e^{\pm nbx}}{\sqrt{\sigma^4 + 4i\kappa\sigma\beta\gamma n^2 b^2}} \left[\frac{\sinh e_1(h-y)}{\sinh e_1 h} - \frac{\sinh e_2(h-y)}{\sinh e_2 h} \right] \right|$$

is of the order $1\cdot8\times10^{8}\times e^{10^{-5}y}\times e^{-10^{-6}nx}$. Hence, the latter is far greater than the former in numerical value. Consequently, the expression (14) for ψ reduces to

$$\psi=\Im\left\{C\gamma e^{i\sigma t}\sum_{n=1}^{\infty}(-1)^{n+1}e^{\pm nbx}\frac{\kappa inb}{\sqrt{\sigma^4+4i\kappa\sigma\beta\gamma n^2b^2}}\times\left[\frac{\sinh e_1(h-y)}{\sinh e_1h}-\frac{\sinh e_2(h-y)}{\sinh e_2h}\right]\right\} \tag{16}$$

where, of the double sign, positive sign should be taken for $x\leqq0$, negative sign for $x\geqq0$, and for e_1 and e_2 see (14′).

Similarly, the expression (15) for ϑ reduces to

$$\vartheta=\pm\Re\left\{Ce^{i\sigma t}\sum_{n-1}^{\infty}(-1)^{n}e^{\pm nbx}\frac{\kappa\sigma}{\sqrt{\sigma^4+4i\kappa\sigma\beta\gamma n^2b^2}}\times\left[(n^2b^2+e_1^2)\frac{\sinh e_1(h-y)}{\sinh e_1h}-(n^2b^2+e_2^2)\frac{\sinh e_2(h-y)}{\sinh e_2h}\right]+F(y,\,t)\right\} \tag{17}$$

where, when $x\leqq0$, positive sign should be taken and $F(y,\,t)=0$; when $x\geqq0$, negative sign and

$$F(y,\,t)=iCe^{i\sigma t}\frac{\sin\left\{\sqrt{\frac{\sigma}{2\kappa}}e^{-i\frac{\pi}{4}}(h-y)\right\}}{\sin\left\{\sqrt{\frac{\sigma}{2\kappa}}e^{-i\frac{\pi}{4}}h\right\}}.$$

To calculate the velocity of the fluid u and v, the series diverges. So we must first calculate the values of ψ at different points in the fluid at any fixed instant, and calculate the values of $\partial\psi/\partial y$ and $\partial\psi/\partial x$ numerically.

III. Application of the Mathematical Solution to the Tank Experiment.

To repeat the meanings of the symboles used, y is the height measured from the bottom of the tank; x the horizontal distance measured from the discontinuity at the bottom, the heated half being taken as positive. Θ is the temperature at any point in the initial state; ϑ the deviation of temperature from Θ after the heating had started. The temperatures in the lowest layer of the fluid are given by the expression (6) in the preceeding Chapter, or by

$$\vartheta_{y=0} = \frac{C}{2} \sin \sigma t \left[\tanh \frac{bx}{2} + 1 \right]. \qquad ((1))$$

Although the heating was not done periodically in the experiments described in Chapter I, the foregoing expression approximately represents the conditions of the experiments. The temperature distributions given by the three curves in Fig. 4 are expressed by ((1)) by putting $b = 0{\cdot}1$. C and σ should be determined from the inclinations of the curves in Fig. 3. If we put $\sigma = 1{\cdot}75 \times 10^{-3}$ (assuming the period of heating and cooling arbitrarily to be one hour), C becomes 1·0 deg. In Fig. 4 we see that the center ($x = 0$) of the 'tanh' curve moves to right gradually with time. This is consistent with that the center of the elliptic stream lines shifts towards the heated half. As the coefficient of expansion of water α is about $1{\cdot}75 \times 10^{-4}$ in the range of temperature used in the experiments, $\gamma = g\alpha = 0{\cdot}17$. In the experiments described in Chapter I, the initial temperature gradient in vertical direction β was 0·111 deg/cm.

Since the calculated height of the calm layer at which the horizontal velocity u becomes null varies greatly with the assumed value of the diffusibility of temperature in vertical direction κ, it seems plausible to determine the value of κ as the calculated height of the calm layer to coincide with the height observed in the experiment. Such value of κ in the present case is 23·8, which value is very much greater than

that measured in still water, and which is only natural, seeing that the superposed vertical convectional currents convey heat.

As e_1 and e_2 given in (14′) in the preceeding Chapter are complex quantities, they are separated into real and imaginary parts, namely

$$e_1 = \mu_1 + i\nu_1, \quad e_2 = \mu_2 - i\nu_2 \qquad ((2))$$

Since y/h is sufficiently small compared to unity in the case when the lowest elliptical circulation alone is considered (h is the depth of the water), the following simplified expression of the stream function ψ may be used in place of expression (16):

$$\psi = C\sqrt{\frac{\kappa\gamma}{2\beta\sigma}} \sum_{n=1}^{\infty} (-1)^{n+1} \left\{ e^{-\mu_1 y} \sin\left(\sigma t + \frac{\pi}{4} - \nu_1 y\right) - e^{-\mu_2 y} \sin\left(\sigma t + \frac{\pi}{4} + \nu_2 y\right) \right\} e^{\pm nbx} \qquad ((3))$$

where n is a positive integer 1, 2, 3, ..., and, of the double sign, the positive sign should be taken for $x < 0$ and the negative for $x > 0$.

Evaluating e_1 and e_2, we get those shown in Table I.

Table I. e_1 and e_2

n	μ_1	ν_1	μ_2	ν_2
1	0·0926	0·257	0·222	0·107
2	0·123	0·388	0·287	0·166
3	0·142	0·503	0·320	0·223
4	0·155	0·612	0·334	0·285
5	0·166	0·718	0·336	0·354
—	—	—	—	—

As $\partial\psi/\partial y$ does not converge for a small value of y, it is impossible to calculate it directly. To find the velocities of the fluid, the values of ψ for different values of y must first be calculated, after which $\partial\psi/\partial y$ can be found as the inclination of a ψ-y curve.

In this way, the values of $\partial\psi/\partial y$ at different heights at $x = 0$ at the times $\sigma t = 80^\circ$ (*i. e.* $t = 13^m\ 20^s$) and $\sigma t = 120^\circ$ (*i. e.* $t = 20^m\ 0^s$) were calculated and plotted in Fig. 14. These curves are quite similar to the observed u-y curves at $10^m\ 30^s$ and $14^m\ 0^s$ shown in Fig. 2, except in the lowest 1·5 cm., where the observed curves are strongly bent by frictional resistance of the bottom. The scale of the velocity, however, greatly exceeds the calculated curves. This discrepancy is clearly due

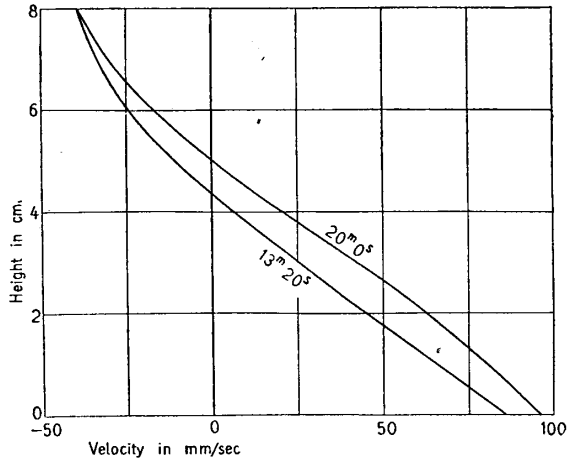

Fig. 14.

to resistance induced by the viscosity of the fluid constantly acting to retard the development of circulation, so that the actual velocities of the fluid are obtained by multiplying the calculated values with a factor F; $F = 0{\cdot}062$ in the present case.

Factor F, however, may vary to some extent with the development of the circulation. We shall at all events assume it to be constant here, and multiply the right side of the expression ((3)) with this factor F in order to have it express the actual motion of the fluid in the experiment.

Table II shows some of the values of $\psi \times F$ calculated by ((3)) using the values of μ and ν given in Table I and using the constants, F=0,062, $C = 1{\cdot}0$, $\kappa = 23{\cdot}8$, $\gamma = 0{\cdot}17$, $\beta = 0{\cdot}111$, $\sigma = 1{\cdot}75 \times 10^{-3}$, and $b = 0{\cdot}10$.

TABLE II. $\psi \times F$.

$\sigma t = 0$

y in cm. \ x in cm.	0	10	20	30	40
2	−0·642	−0·451	−0·216	−0·089	−0·038
5	−1·372	−0·974	−0.451	−0·184	−0·070
10	−1·613	−1·088	−0·419	- 0·159	−0·057
15	+0·153	+0 044	−0·019	−0·013	−0·006

$\sigma t = \frac{\pi}{4}$

y in cm. \ x in cm.	0	10	20	30	40
2	+0·286	+0·165	+0·076	+0·025	+0·006
5	+0·248	+0·134	+0·006	−0·006	−0·004
10	−1·080	−0·722	−0·311	−0·121	−0·044
15	−0 775	−0·476	−0·153	−0·051	−0·019

$\sigma t = \frac{\pi}{2}$

y in cm. \ x in cm.	0	10	20	30	40
2	+1·023	+0·750	+0·337	+0·140	+0·051
5	+1·360	+0·930	+0·382	+0·153	+0·057
10	+0·063	+0·038	+0·019	+0·013	+0·006
15	−0·706	−0·464	−0·165	−0·057	−0·091

$\sigma t = \frac{\pi}{2} + \frac{\pi}{4}$

y in cm. \ x in cm.	0	10	20	30	40
2	+1·212	+0·852	+0·394	+0·159	+0·063
5	+1·905	+1·340	+0·591	+0·235	+0·089
10	+1·245	+0·800	+0·286	+0·095	+0·038
15	−0·273	−0·165	−0·083	−0·032	−0·013

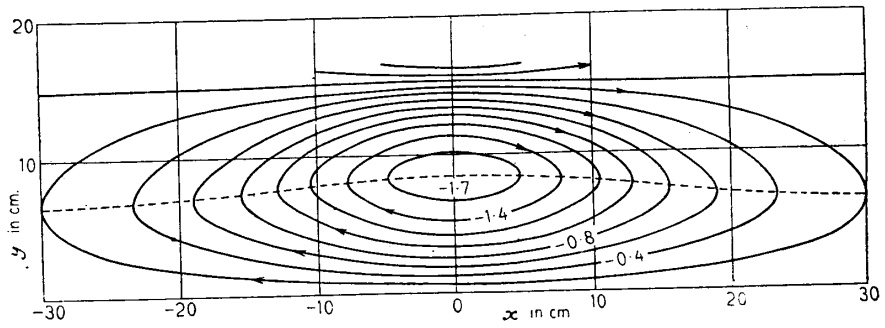

Fig. 15. $\sigma t = 0$.

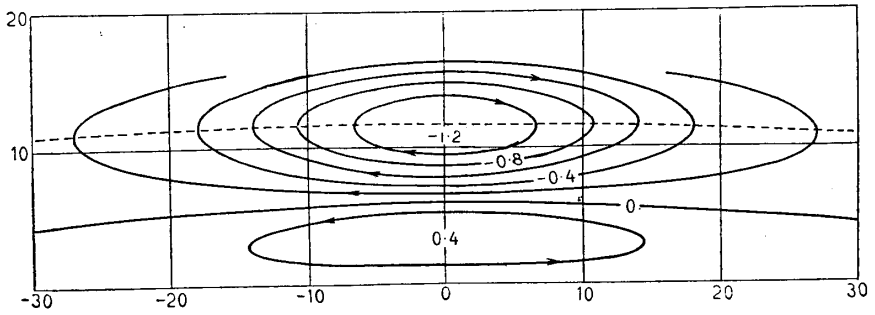

Fig. 16. $\sigma t = \frac{\pi}{4}$.

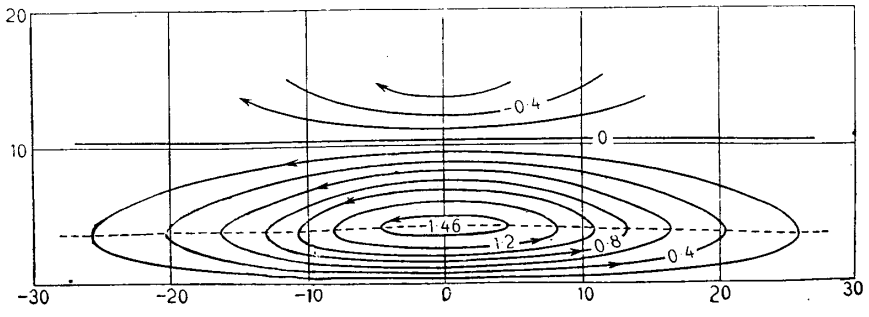

Fig. 17. $\sigma t = \frac{\pi}{2}$.

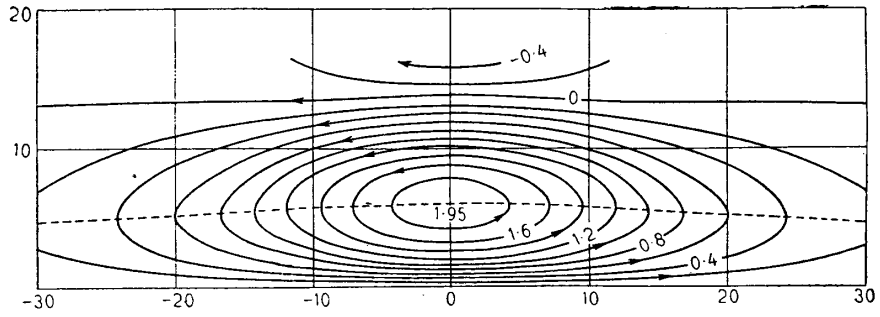

Fig. 18. $\sigma t = \frac{3\pi}{4}$.

The values of $\psi \times F$ at different phases are shown graphically in Fig. 15, 16, 17, and 18. At $\sigma t = 0$, the circulation that had developed during the period in which the right hand side half of the bottom was cooled retains its activity. At $\sigma t = \pi/4$, we see that a small circulation has already started as the result of the heating of the right half of the bottom. This circulation, which grows energitic with time, attains its maximum velocity at a time between $\sigma t = \pi/2$ and $\sigma t = 3\pi/4$. The height of the circulation (or the height of the calm layer) increases with time, even after $\sigma t = \pi$.

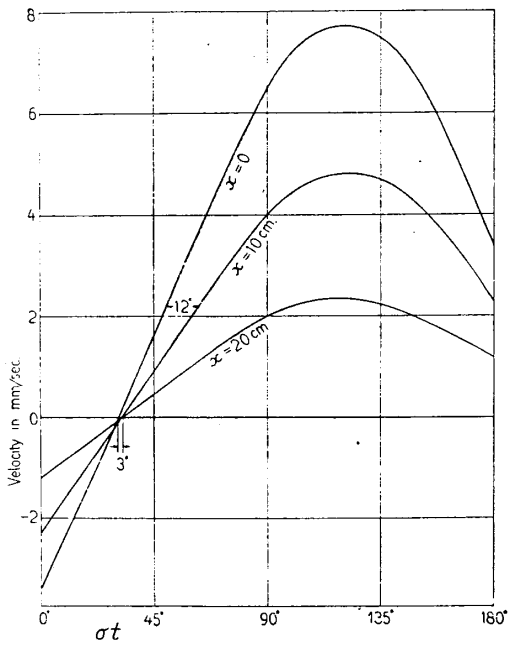

Fig. 19.

We shall consider next the rate of extension of the elliptic circulation to both positive and negative directions of x. Fig. 19 shows the variations with time in the calculated velocities of the fluid in the lowest layer at points $x=0$, $x=10$ cm., and $x=20$ cm. As the distance at which the curves for $x = 0$ and $x = 10$ cm.

intersect with the time-axis is about 3°, or 30 seconds of time, the mean velocity of extension of the circulation in x-direction between $x = 0$ and $x = 10$ cm. is 3·3 mm/sec. This velocity increases rapidly with development of circulation.

The velocity of extension of the circulation just given, is much greater than the observed propagational velocity of the circulation-front on the heated half of the bottom, which latter is 0·84 mm/sec. This can be interpreted to mean that, on the heated half of the bottom the elliptical circulation must force its way through the vertical convectional currents present in order to extend its domain, with result that a certain finite amount of dynamical pressure is necessary for the advancement of its front. It will be seen from Fig. 19 that the propagational velocity of the phase of $u = 2{\cdot}2$ mm/sec. is about 0·84 mm/sec., so that it is possible to estimate the dynamical pressure necessary at the front to be of the order corresponding to this velocity, namely, 2·2 mm/sec. The velocity of the 2·2 mm/sec. is approximately in agreement with the observed velocity of fluid in the neighbourhood of the front.

The mathematical solution illustrates well the motion of the fluid on the cold half of the bottom when the other half of the bottom was heated, and on both halves of the bottom when half of the bottom was cooled.

IV. Application of the Mathematical Solution to Problems of Land and Sea breezes.

The wind conditions at various heights were measured on July 15, 1930, by means of pilot-baloons at the former site of the Aeronautical Research Institute in Ettyûzima that lies on the coast of the city of Tokyo. The baloons were observed at two stations 679 m. apart. It was a very fine and sunny day; the gradient wind was low, except for an abnormal lull and blow that occurred during the period from 14^h to 20^h, (See Fig. 28) caused probably by a small passing depression. A

mild easterly wind that prevailed in the morning died out by 14^h. Above 1500 m., a strong NE wind blew all day.

The paths of the three baloons, that were released at 11^h, 13^h, and 15^h, are shown in Fig. 20. The components of the wind perpendicular to the coast line, found from Fig. 20, vary with height as shown in

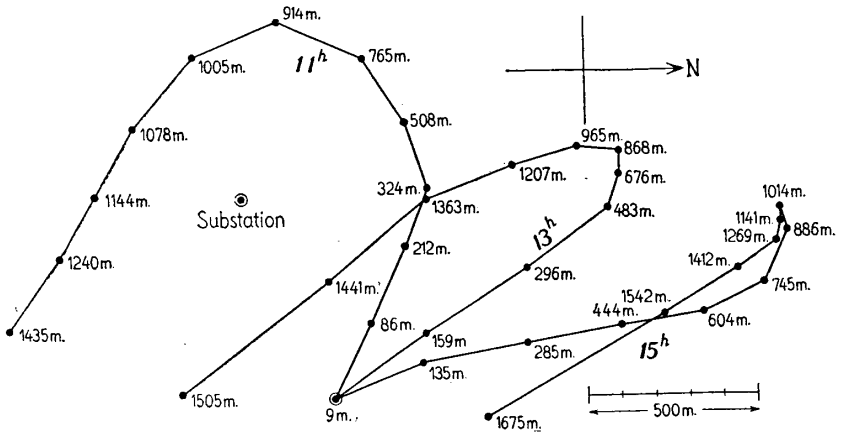

Fig. 20. Black circle shows the position of the ballon at the end of each minute; the height is marked thereby.

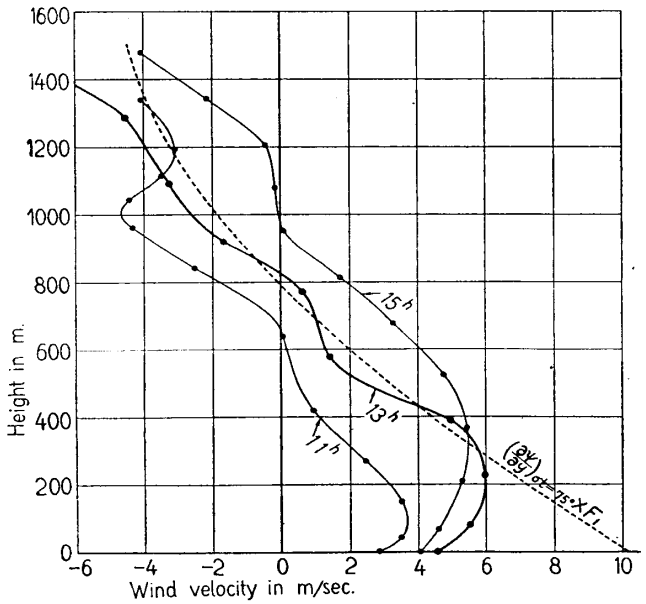

Fig. 21.

in Fig. 21. Of the three, the result for 13^h will now be compared with the mathematical solution.

Since y/h in the case of land and sea breezes is also sufficiently small compared with unity (h is the height of the homogeneous atmosphere in this case), the expression for the stream-function ψ may be used in the simplified form written below, the same as ((3)) in the preceding Chapter.

$$\psi = C\sqrt{\frac{\kappa\gamma}{2\beta\sigma}}\sum_{n=1}^{\infty}(-1)^{n+1}\left\{e^{-\mu_1 y}\sin\left(\sigma t+\frac{\pi}{4}-\nu_1 y\right)\right.$$
$$\left.-e^{-\mu_2 y}\sin\left(\sigma t+\frac{\pi}{4}+\nu_2 y\right)\right\}e^{\pm nbx} \qquad ((3))$$

where x is the distance from the coast line, the direction inland being positive, and y the vertical height above the earth's surface. β is the vertical gradient of the potential temperature, which may be assumed to be $3{\cdot}5\times10^{-5}$ deg/cm., while γ stands for $g\alpha$ (g being the acceleration of gravity and α the thermal expansion coefficient of air), whence $\gamma = 980/273 = 3{\cdot}59$. For μ and ν see ((2)) in Chapter 3 and (14′) in Chapter 2. C, σ and b are to be determined from expression ((1)), which gives the distribution and variation in temperature ϑ on the earth's surface, or

$$\vartheta_{y=0} = \frac{C}{2}\sin\sigma t\left[\tanh\frac{bx}{2}+1\right]. \qquad ((1))$$

As the period of variation in temperature is 24 hours, $\sigma = 7{\cdot}28\times10^{-5}$. We see from the temperature record in Fig. 22 that the mean temperature, which was 28·8°, occurred at 8^h, and the maximum temperature, which was 32·2°, was attained at 14^h. Therefore we have $C = 6{\cdot}8$ deg., and t should be measured from 8^h.

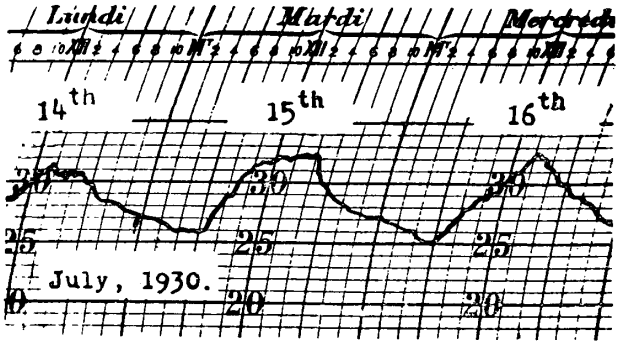

Fig. 22.

Fig. 23 shows the mean diurnal veriation of temperature of all fine days in July during the period from 1926 to 1930, according to which diagram, we have $C = 7{\cdot}0$, deg., and $8^h\ 30^m$ as $t = 0$.

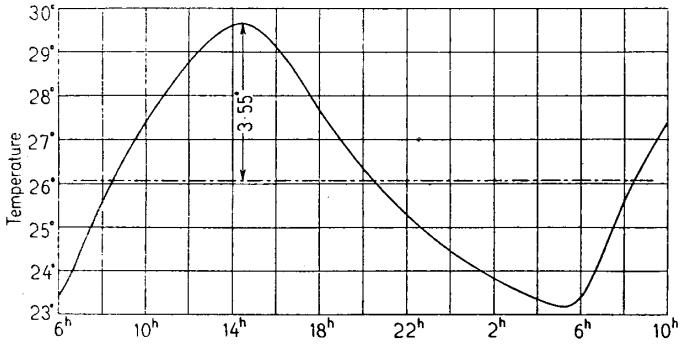

Fig. 23. Mean temperature of 25 fine days in July, 1926—1930.

There being no meteorological observatory at a convenient distance from the Institute, we lack the datum for determining b. We shall therefore assume that the sea has practically no daily influence on the atmospheric temperature at 40 km. from the coast, or $\tanh \frac{bx}{2} \approx 1$ at $x = 40$ km. We then have $b = 10^{-6}$.

At Kumagaya observatory, 65·5 km. from the Institute in which direction the sea-breezes usually blow, the temperature at 14^h on the same day was 34·5°, which is 2·3° higher than the temperature at the same time at the Institute. Substituting this value in ((1)), we get $b = 2{\cdot}5 \times 10^{-7}$, which value, however, is evidently too small, seeing that

on this assumption the effect of the sea-breeze will be felt 150 km. inland.

Another constant κ, the diffusibility of temperature in vertical direction, should be determined, as in the preceeding Chapter, as the calculated height of the calm layer to coincide with the observed height, which is about 800 m. at 13^h (see Fig. 21). The procedure, however, is laborious, because a suitable value of κ can be found only after repeated calculations of the height at which ψ becomes maximum for each value of κ tentatively adopted. In the present case, maximum of ψ at 13^h works out to 800 m. (792 m. to be exact) when the assumed $\kappa = 4{\cdot}5 \times 10^7$. This value of κ greatly exceeds that found by G. I. Taylor, which, however, is not surprising, seeing that in the case of convectional circulation, the superposed vertical convectional currents play a much more important rôle in carrying heat in a vertical direction than the mixing of air as the result of eddy motion.

Table III shows the values of e_1 or $\mu_1 + i\nu_1$ and e_2 or $\mu_2 - i\nu_2$ for each n, calculated by assuming that $\kappa = 4{\cdot}5 \times 10^7$ and $b = 10^{-6}$.

TABLE III.

n	$e_1 \times 10^5$	$e_2 \times 10^5$
1	0·53684 + i 1·2973	1·2885 − i 0·53424
2	0·75541 + i 1·8386	1·8183 − i 0·75937
3	0·92208 + i 2·2571	2·2216 − i 0·93321
4	1·06161 + i 2·6127	2 5588 − i 1·0808
5	1·1836 + i 2·9283	2·8535 − i 1·2118
6	1·2932 + i 3·2158	3·1178 · i 1·3312
7	1·3931 + i 3·4820	3·3589 − i 1·4418
8	1·4855 + i 3·7317	3·5815 − i 1·5455
9	1·5716 + i 3·9678	3·7888 − i 1·6437
10	1·6524 + i 4·1927	3·9833 − i 1·7373
11	1·7287 + i 4·4081	4·1666 − i 1·8270
12	1·8011 + i 4·6154	4·3404 − i 1·9134
13	1·8701 + i 4·8156	4·5056 − i 1·9969
14	1·9359 + i 5·0095	4·6632 − i 2·0779
15	1·9989 + i 5·1979	4·8139 − i 2·1567
—	—	—

Table IV shows the values of ψ at 13^h or $\sigma t = 75^\circ$ at various heights at $x = 0$, calculated by means of expression ((3)) by using the values of μ and ν given in Table III, and the values of $\partial\psi/\partial y$, (which give the wind velocities in cm/sec.) obtained by measuring the inclinations of the ψ-y curve.

TABLE IV. ψ and $\partial\psi/\partial y$ at $\sigma t = 75^\circ$ and at $x = 0$.

Height in m.	$\psi \times 10^{-5}$	$\partial\psi/\partial y$
0	0	7170
100	667	6060
200	1233	5030
300	1694	4040
400	2034	3060
500	2280	2200
600	2455	1395
700	2558	655
800	2588	− 55
900	2548	− 705
1000	2446	−1310
1100	2292	−1820
1200	2086	−2280
1300	1839	−2655
1400	1558	−2945
1500	1253	−3150

The wind velocities $\partial\psi/\partial y$ in the above table are much greater than those actually observed, which, as mentioned in the preceeding Chapter, is evidently the result of the assumption that the fluid is inviscid. They are the volocities of a circulation developed without any resistance. Since, however, circulation in ordinary fluid grows under unceassing resistance due to viscosity, the velocities of the actual winds can readily be obtained by multiplying the values of $\partial\psi/\partial y$ in Table IV with a certain factor. Since the wind in the lowest layer is subdued by the resistance of the eath's surface, we shall assume that the wind attains the necessary velocity for circulation at a height of 300 m. As the observed wind velocity at 300 m. was 5·73 m/sec. (See Fig. 21), the factor to be multiplied with $\partial\psi/\partial y$ is

$$F_1 = 573/4040 = 0{\cdot}1418 .$$

The wind velocities at various heights obtained by multiplying $\partial\psi/\partial y$ with F_1 are plotted in Fig. 21 with a dotted line.

If we assume $b = 2{\cdot}5 \times 10^{-7}$, taking into account the temperature at Kumagaya, the value of κ, which makes the calculated height of the calm layer 800 m. at 13^h, becomes $\kappa = 3 \times 10^6$. The values of $\partial\psi/\partial y$ come out much smaller (nearer to the actual wind velocities) than the corresponding values in Table IV; for example 1730 cm/sec. at $y = 0$. However, since assuming b to be smaller would mean estimating the gradient of the temperature on the earth's surface to be smaller, it is obvious that the smaller the-resulting value of b, the slower the development of convectional circulation. In fact, $b = 10^{-6}$ would be better.

It will be seen from Fig. 21 that the wind velocity curves are bend towards the smaller velocity value in the lowest 300 or 400 m., which obviously is owing to frictional resistance of the surface of the earth or the sea. Therefore, in order to find the wind velocity in the lowest layer, the calculated wind velocity or $(\partial\psi/\partial y) \times F_1$ must be multiplied by another factor F_2. As the measured wind velocity on the earth's surface at 13^h was 4.55 m/sec., we get

$$F_2 = \frac{455}{7170 \times 0{\cdot}1418} = 0{\cdot}448 .$$

This is somewhat smaller than the ratio of actual wind on the earth's surface to the calculated velocity of the gradient wind, which is 0.5—0.6 on a flat land surface. There is no doubt that F_2 is still smaller inland.

The factor F_1, the ratio of the circulations developed with and without resistance, may vary to some extent with the stage of development of the circulation. In the following discussions, however, both F_1 and F_2 are assumed to be constant.

Table V shows some values of ψ at different heights and at different distances from the coast at 8^h, 11^h, 14^h, and 17^h, calculated by assuming $\kappa = 4{\cdot}5 \times 10^7$, $b = 10^{-6}$, $\gamma = 3{\cdot}59$, $\beta = 3{\cdot}5 \times 10^{-5}$, $\sigma = 7{\cdot}28 \times 10^{-5}$, and $C = 6{\cdot}8$.

Table V. $\psi \times 10^{-5}$

$\sigma t = 0$

y in m.	$x = 0$	2 km.	5 km.	10 km.	20 km.
500	−1701	−1584	−1382	−1201	−488
1000	−3105	−2842	−2427	−1763	−796
1500	−3870	−3455	−2851	−1973	−834
2000	−3781	−3250	−2553	−1655	−644

$\sigma t = \frac{\pi}{4}$

y in m.	$x = 0$	2 km.	5 km.	10 km.	20 km.
500	+ 787	+ 699	+ 568	+ 389	+ 157
1000	+ 170	+ 84	− 15	− 94	− 86
1500	−1100	−1071	− 977	− 765	− 368
2000	−2217	−2009	−1682	−1176	− 497

$\sigma t = \frac{\pi}{4}$

y in m.	$x = 0$	2 km.	5 km.	10 km.	20 km.
500	+2788	+2570	+2186	+1585	+713
1000	+3342	+2957	+2406	+1632	+673
1500	+2330	+1951	+1469	+ 888	+314
2000	+ 396	+ 156	− 29	− 150	−121

$\sigma t = \frac{\pi}{2} + \frac{\pi}{4}$

y in m.	$x = 0$	2 km.	5 km.	10 km.	20 km.
500	+3226	+2900	+2510	+1856	+ 849
1000	+4562	+4108	+3417	+2403	+1039
1500	+4372	+3789	+3061	+2022	+ 810
2000	+3063	+2552	+1917	+1161	+ 415

The variations in ψ with height at $x = 0$ at different phases are plotted in Fig. 24. Measuring the inclinations of these curves, we obtain $\partial\psi/\partial y$, some of which are shown in Table VI.

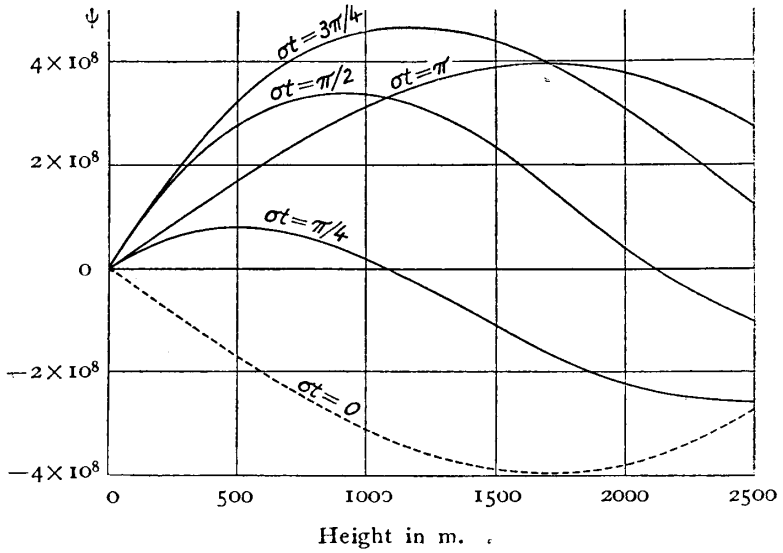

Fig. 24.

TABLE VI. Wind velocity (calculated) in m/sec. at $x = 0$,

or $\left(\frac{\partial\psi}{\partial y}\right)_{x=0} \times F_1 \div 100$

Height in m.	$\sigma t = 0$	$\sigma t = \pi/4$	$\sigma t = \pi/2$	$\sigma t = 3\pi/4$
0	−5·09	+4·86	+11·89	+12·17
250	−4·86	+2·12	+ 8·34	+ 9·37
500	−4·49	0·00	+ 4·95	+ 6·59
750	−3·96	−1·78	+ 1·79	+ 3·97
1000	−3·22	−3·12	− 1·10	+ 1·56
1250	−2·24	−3·71	− 3·33	− 0·67
1500	−0·97	−3·73	− 4·88	− 2·51
1750	+0·38	−3·18	− 5·41	− 3·95
2000	+1·68	−2·26	− 5·01	− 4·91

The variation in the calculated wind velocity with height on the coast line are plotted in Fig. 25. It will be seen from this diagram how the height of the calm layer increases with development of circulation. At a point away from coast, the wind varies with height and with time

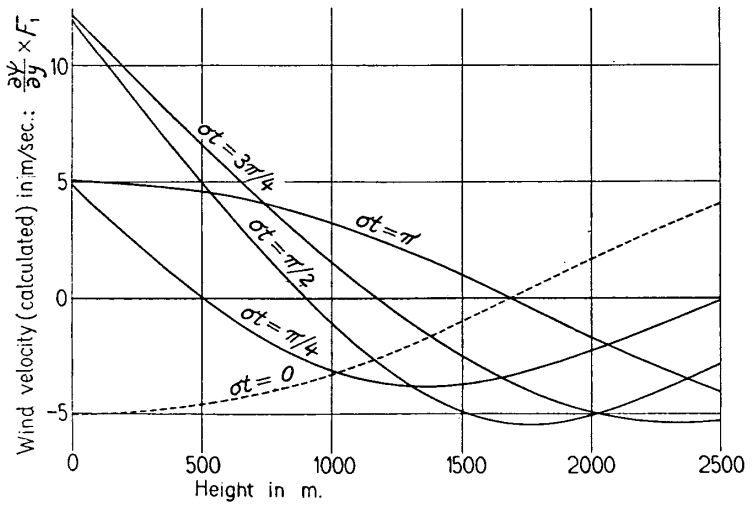

Fig. 25.

in nearly the same way as on the coast, but both wind velocity and vertical scale are smaller than those at the coast. The heights of the calm layer at $x = 0$ and $x = 10$ km. change with time as shown in Table VII.

TABLE VII. Height of calm layer (calculated) in m.

	$\sigma t = \pi/4$	$\sigma t = \pi/2$	$\sigma t = 3\pi/4$	$\sigma t = \pi$
$x = 0$	500	900	1170	1675
$x = 10$ km.	420	760	1000	1410

The wind velocities in the lowest layer at different phases of development and at varying distances from the coast are given in Table VIII. To calculate $\partial\psi/\partial y$ at $y = 0$, the values of ψ at heights 100, 200, 300, 400, and 500 m. were calculated, the algebraical relation $\psi = ay + by^2 + cy^3$

being then assumed, and coefficient a was found by the method of least squares.

TABLE VIII. Wind velocity (calculated) on the earth's surface in m/sec.,

or $\left(\frac{\partial \psi}{\partial y}\right)_{y=0} \times F_1 \times F_2 \div 100$

σt	$x = 0$	2 km.	5 km.	10 km.	20 km.
0°	−2·28	−2·16	−1·89	−1·40	−0·65
30°	+0·81	+0·71	+0·63	+0·47	+0·21
60°	3·57	3·24	2·83	2·19	1·07
90°	5·32	5·02	4·40	3·30	1·59
120°	5·77	5·37	4·69	3·59	1·69
150°	4·61	4·32	3·74	2·86	1·38

The results given in Table VIII are plotted in Fig. 26.

The variation in the calculated velocity on the coast with time will now be compared with the observed results of the actual wind. As will

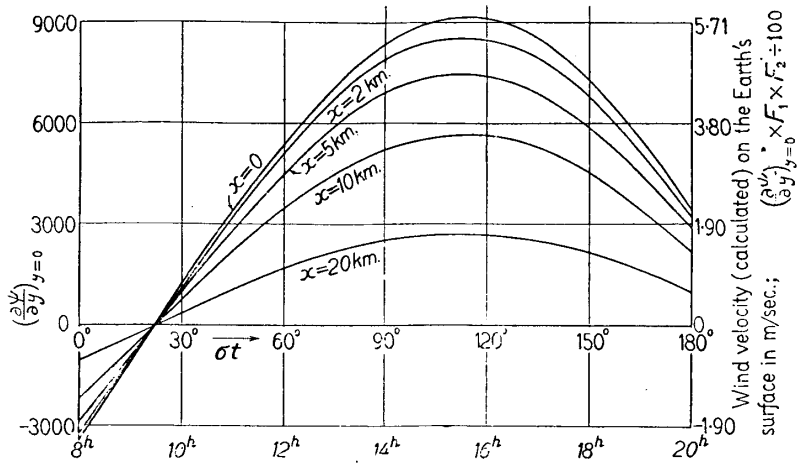

Fig. 26.

be seen from the record reproduced in Fig. 27, the wind veered from land to sea during the lull from 10h to 10h 20m. The variations in the

observed wind velocities are shown in Fig. 28. The plain circles are the mean velocities of the wind for 20 minutes each on July 15, 1930, as

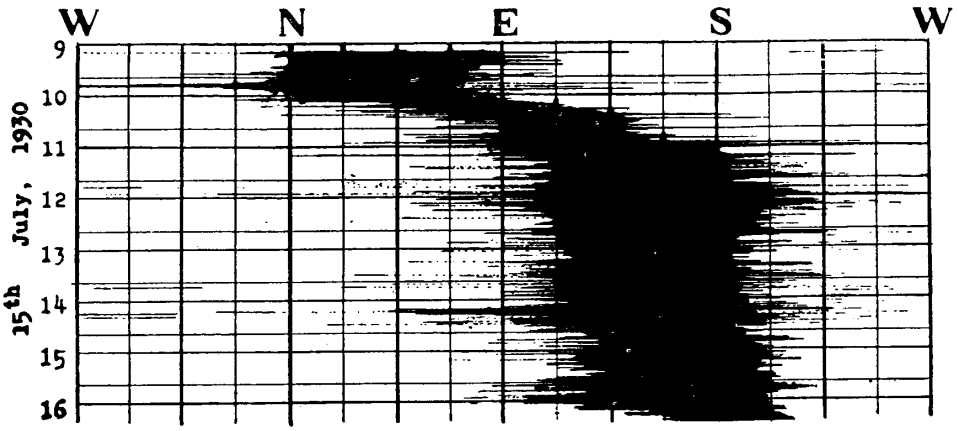

Fig. 27.

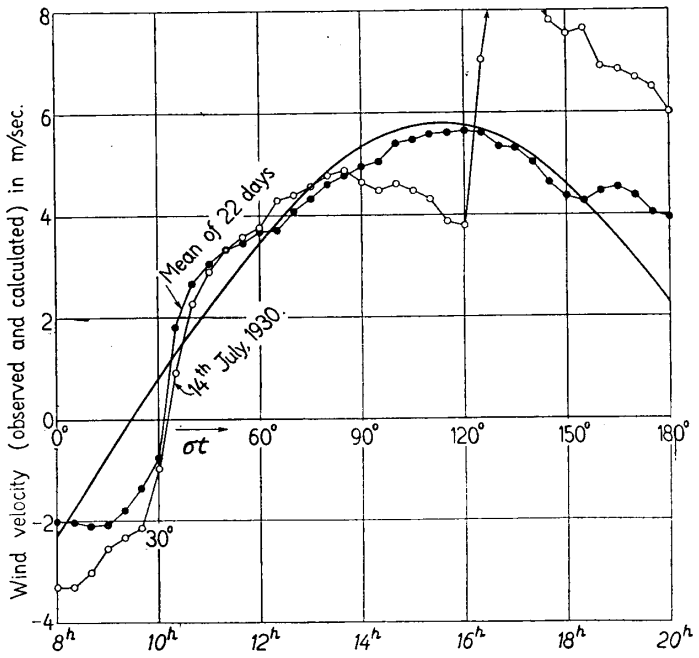

Fig. 28.

measured by the Robinson anemometer installed on the roof of the Institute, the values before 10h being taken as negative and after 10h

20^m as positive. The black circles show the average of similar velocities of 22 selected days—all fine days with small gradient winds in June and July during the period from 1926 to 1930. The signs were determined with reference to the records of wind direction of the corresponding days. Except in the neighbourhood of the point where the curve cut the time-axis, both curves are quite consistent with the calculated curve. The values of actual wind velocities greater (absolute) than the calculated values in that part are partly caused by superposition of the prevailing wind in a direction with the component parallel to the coast line, although it is quite evident that reversal in direction of the wind is much more abrupt than what the calculation shows, which is to be expected from our experience with the tank experiment. If the points at which the calculated velocity-time curve of the surface-wind shown in Fig. 26 cut the time-axis are found, the velocity of propagation of the phase $(\partial\psi/\partial y)_{y=0} = 0$ from the coast in directions both inland and out to sea can be determined. The curves between $\sigma t = 15^\circ$ and 35° were very accurately drawn by calculating the values of $\partial\psi/\partial y$ for small intervals. As the result of which it was found that the curves for $x = 0$, $x = 5$ km., $x = 10$ km., and $x = 20$ km. cut the time-axis at $\sigma t = 22^\circ 3'$, $22^\circ 20'$, $22^\circ 29'$, and $22^\circ 44'$ respectively. We therefore obtain 73·5, 139, and 167 m/sec. as the mean velocities of propagation between $x = 0$ and 5 km., 5 km. and 10 km., and 10 km. and 20 km. respectively. If the propagating velocity of the boundary of the circulation are so great, the breeze will cover the entire area over which it blows within a few minutes from its start from the coast. This seems to be nearly the truth in the case of land breezes and on the sea in the case of sea breezes, although the velocity of propagation inland in the case of sea breezes is much smaller. It is known that sea breezes start at a point on the sea a few kilometers off the coast nearly simultaneously with that on the coast. Photo 7 shows that the circulation extends much quicker on a cold than on a heated bottom. As mentioned in the preceeding Chapter, we may assume that a certain finite amount of dynamical

pressure is necessary to convectional circulation in order that its boundary shall be extended through space which is full of vertical convectional currents. Fig. 28 shows that starting of the sea breezes on the coast lags about 40 minutes from the time as shown by calculation and springs up abruptly with a velocity of from 1 to 2 m/sec. By assuming the velocity of the sea breezes in the neighbourhood of its front (or the velocity immediately after it has begun to blow), we can estimate from Fig. 26 the time-lag in its starting and its velocity of propagation, as shown in Table IX.

Table IX

Assumed wind velocity on front	At $x = 0$, sea-breeze starts at	Mean propagational velocity of front in the range $x =$		
		0—5 km.	5 km.—10 km.	10 km.—20 km.
0	9h 28m	73·5 m/sec.	139 m/sec.	167 m/sec.
1 m/sec.	10h 9m	9·05 „	3·88 „	2·03 „
2 m/sec.	10h 52m	4·34 „	0·86 „	—

Seeing from the results, assumption of 1 m/sec. seems to be nearly correct.

Since the calm layer is much lower in the case of land-breezes, the value of κ must be smaller than that in the case of sea breezes, and perhaps agree with the Taylor's value.

In order to arrive at further conclusions it is necessary to measure accurately the distributions of temperature and the propagational velocity of the sea-breeze front.